

ADDRESSING SELECTION BIAS AND MEASUREMENT ERROR IN COVID-19 CASE COUNT DATA USING AUXILIARY INFORMATION

WALTER DEMPSEY

ABSTRACT. Coronavirus case-count data has influenced government policies and drives most epidemiological forecasts. Limited testing is cited as the key driver behind minimal information on the COVID-19 pandemic. While expanded testing is laudable, measurement error and selection bias are the two greatest problems limiting our understanding of the COVID-19 pandemic; neither can be fully addressed by increased testing capacity. In this paper, we demonstrate their impact on estimation of point prevalence and the effective reproduction number. We show that estimates based on the millions of molecular tests in the US has the same mean square error as a small simple random sample. To address this, a procedure is presented that combines case-count data and random samples over time to estimate selection propensities based on key covariate information. We then combine these selection propensities with epidemiological forecast models to construct a *doubly robust* estimation method that accounts for both measurement-error and selection bias. This method is then applied to estimate Indiana’s active infection prevalence using case-count, hospitalization, and death data with demographic information, a statewide random molecular sample collected from April 25–29th, and Delphi’s COVID-19 Trends and Impact Survey. We end with a series of recommendations based on the proposed methodology.

1. INTRODUCTION

The World Health Organization has declared the coronavirus disease 2019 (COVID-19) a public health emergency. As of July 29th, 2021, over 196 million cases have been confirmed worldwide with 34.8 million cases and over 612 thousand confirmed deaths across the United States. This pandemic has become the focal point of everyday life; yet the data landscape for understanding COVID-19 remains limited. Public databases [Dong et al., 2020, Smith et al., 2020] provide incoming county-level information of confirmed cases and deaths. Statisticians, epidemiologists, economists, and data scientists have used this granular data to forecast COVID-19 case-counts, deaths, and hospitalizations [Giordano et al., 2020, Song et al., 2020, Ray et al., 2020, IHME and Murray, 2020, Wang et al., 2020, Yang et al., 2020].

This paper has two main objectives. The first objective is to express reservations at the use of observed case-counts as a proxy for disease prevalence and in estimation of standard epidemiological models for inference and forecasting. The reason is straightforward: observed case-count data is plagued by selection bias and measurement error. Through a series of calculations, we will demonstrate that the information gained from increasing testing capacity is limited in the presence of selection bias and when testing inaccuracies persist. In particular, the millions of tests in the US have a small effective sample size when compared to random sampling. These calculations demonstrate the importance of probabilistic sampling designs over time for estimation of point prevalence and effective reproduction number.

Selection bias in case-count data is primarily due to it being a *diagnostic tool*, i.e., individuals who are symptomatic or have a known/suspected exposure are more likely to present for diagnostic testing. Case-count data arising from non-random testing means it cannot provide valid prevalence or incidence estimates due to the significant proportion of asymptomatic and pauci-symptomatic cases. Random testing, on the other hand, is used for *screening purposes*, i.e., is an appropriate tool for reconstructing prevalence/incidence estimates. Due to monetary and time constraints, however, random testing is performed infrequently. As of June 2021, Indiana and Ohio are the only states to conduct statewide random sample testing¹. Indiana’s sample was collected from April 25–29, 2020 [Yiannoutsos et al., 2021]. Such infrequent random testing is likely to provide insufficient

¹These are the only random samples to collect both seroprevalence and diagnostic testing results. The CDC and other states have conducted seroprevalence-only studies.

information to help researchers and policy makers better understand the disease trajectory which can change rapidly over time. Therefore, while random testing may be preferable in theory, in practice governments, researchers, and policy makers continue to use coronavirus case-counts to understand the impact of COVID-19 on the population and make data-informed decisions.

The second objective is to demonstrate how random samples provide necessary *auxiliary information* to address selection bias in coronavirus case-count data. Random samples provide the necessary covariate information from a representative sample from the population to estimate selection propensities. These propensities can then be used in an inverse-probability weighting scheme to construct estimators of disease prevalence that attempt to control for selection bias. A doubly robust extension allows researchers to combine these estimates with epidemiological forecasts based on compartmental models that are common in the study of infectious diseases [Hao et al., 2020, Song et al., 2020, Ray et al., 2020, Johndrow et al., 2020].

The proposed approach requires covariate information to be collected on individuals who receive a COVID-19 test. Unfortunately, many states do not require or report auxiliary covariate information beyond basic demographic information (e.g., gender, age, race, and ethnicity). We end with a brief list of suggestions of changes to current practice based on the proposed methodology. While we demonstrate empirical improvements over simple disease prevalence estimates, we also highlight how selection bias may persist and impact uncertainty quantification.

Remark 1 (An evolving pandemic). *This paper focuses on COVID-19 case count, testing, and death data collected from April 2020 through February 2021. Numbers presented on disease dynamics are therefore based on the original strain. Selection bias and measurement error persist in data arising from the delta and omicron strains and will likely persist for future variants. While not discussed in this paper, the framework presented will remain an appropriate tool for addressing selection bias and measurement error in these settings.*

1.1. Related work. This article discusses the relationship between three statistical concepts: selection bias, measurement error, and population size. Potential biases in observational studies of COVID-19 have been identified elsewhere in the literature [Kahn et al., 2021, Accorsi et al., 2021]. While the impact of measurement error [van Smeden et al., 2019] and selection bias [Keiding and Louis, 2016] on estimation are both well-studied topics in general, here we provide a new perspective

by building on the work of Meng [2018] who studied an error decomposition to understand the relationship between selection bias and population size. Specifically, we quantify the interaction between measurement-error and selection bias on statistical error, showing how the sign and magnitude can change drastically. We then discuss this relationship in the context of observational COVID-19 case-count data, showing the impact on the effective sample size can be quite large.

After demonstrating the limitations of case-count analysis when compared to random sampling, we then assess whether there is potential for combining the *nonprobability samples* with *probability samples* to improve point prevalence estimation. For any probability sampling design, the Horvitz-Thompson estimator [Horvitz and Thompson, 1952] incorporates design information via inverse-probability weights (IPW). For nonprobability samples, the IPW estimator requires modelling the propensity scores. Its use in the survey context is also referred to as quasi-randomization [Elliott and Valliant, 2017]. Valliant and Dever [2011] consider a weighted logistic regression procedure using the pooled probability and nonprobability samples. Chen et al. [2019] consider a pseudo-likelihood approach that uses the random samples as a proxy for a term in the log-likelihood. Here, we extend this approach to account for measurement-error as well as observing random samples at multiple times. We then provide an extension of the statistical error decomposition and discuss the trade-offs inherent in such a weighting approach. The proposed approach is distinct from validation studies [Fox et al., 2020] – a traditional epidemiological method in which investigators compare measurement accuracy with a gold standard measure to mitigate bias. Here, the *gold standard* of a different test is replaced by a sample with a less biased selection mechanism.

One core component of coronavirus research is epidemiological compartmental modelling of case-count and death data. These models can be used to answer a variety of research questions including case-count forecasting, estimation of the effective reproduction number, and estimation of quarantine and other health policies on infectious disease dynamics. The basic approach is a deterministic compartmental model called the susceptible-infectious-recovered (SIR) model. A probabilistic extension was proposed by Osthus et al. [2017] to model one-dimensional time series of infected proportions. Song et al. [2020] extended this approach to incorporate interventions and assess interventions on COVID-19 epidemic in China. Hao et al. [2020] extends this work further to

account for various presymptomatic infectiousness, time-varying ascertainment rates, transmission rates and population movements.

Given a probability sampling design, individual predictions can be leveraged to improve estimation via model-assisted approaches [Breidt and Opsomer, 2017]. For nonprobability samples, Chen et al. [2019] derive a doubly robust approach that uses outcome predictions given covariates on the nonprobability and probability samples. Here, we combine the compartmental model of Song et al. [2020] but instead, as in Johndrow et al. [2020], focus on COVID-19 confirmed death count data. We generate epidemiological forecasts for active infection rates within each population strata. We then demonstrate how to combine these forecasts with the IPW approach to construct doubly-robust estimates of active infection rates. A derived statistical error decomposition guides this discussion.

Recent work by Zhao et al. [2021] pointed out that estimation of key epidemiological parameters such as the incubation time using standard epidemiological models can suffer from severe bias due to issues beyond selection bias and measurement error. Right truncation and epidemic growth lead to patients “being more likely to be infected towards the end of their exposure period” [Zhao et al., 2021, pp. 3]. Their approach constructs a study sample and statistical model to account for these issues. In this paper, rather than focusing on sample construction, we ask whether one can collect auxiliary information to address selection bias in the observed case count data directly. Our approach is related to the concept of *target validity* [Westreich et al., 2018], in which the issues of internal and external validity are jointly addressed with respect to a specific population of interest. This article is a concrete attempt to address both types of validity and extend the conversation on target validity within the context of analysis of observational COVID-19 studies.

2. COVID-19 TESTING AND DATA

Here we provide the necessary background to understand COVID-19 diagnostic testing, its scientific use in managing the pandemic, and the data streams considered in this paper.

2.1. Diagnostic testing. Upon infection with the original SARS-CoV-2 variant, an incubation period (time to symptom onset) starts and lasts approximately five days [Lauer et al., 2020]. The viral load will be detectable by at least the end of the latent period (time to infectiousness), which for the original SARS-CoV-2 variant occurs before the end of the incubation period. A *molecular*

test refers to diagnostic tests that aim to detect viral load above a certain threshold (e.g., RT-PCR or antigen tests); see Mina et al. [2020] for a detailed discussion of cycle thresholds. If someone has an active infection – here defined as being infected with SARS-CoV-2 and having a viral load that has yet to fall below detectable levels by RT-PCR testing – then after the incubation period, a molecular test with perfect sensitivity will yield a positive result while the patient has a viral load above the threshold of detection. After that, the viral load will decrease below that threshold and a molecular test with perfect specificity will come back negative. While an individual infected with the original SARS-CoV-2 strain may yield a positive molecular test for several weeks, they will likely stop transmitting the disease within a few days of infection, meaning a positive molecular test does not imply transmissibility.

A molecular test conducted on an actively infected individual may return a negative result. Such false negatives are very strongly associated with when the test is conducted. In the incubation phase, most molecular tests will return a false negative result. Molecular tests are most sensitive when the viral loads are highest which for the original strain occurs during the first few days of transmissibility [Mina et al., 2020]. Moreover, most molecular tests are performed via nasopharyngeal swab. Specimen collection by swab is known to impact false negative/positive rates regardless of test timing. Systematic reviews suggest that 87% sensitivity and 97.6% specificity are reasonable estimates for RT-PCR tests performed during the time window under consideration in this paper [Arevalo-Rodriguez et al., 2020, Woloshin et al., 2020, Cohen et al., 2020]. To the best of our knowledge, both Indiana Department of Health’s molecular testing and the random state-wide RT-PCR tests were primarily collected via nasopharyngeal swab.

The primary goal of molecular tests is diagnosis of active infections in the population. Such diagnostic tests generate important information about the presence of SARS-CoV-2 in the population, and help scientists and policy-makers understand patterns of transmission and propagation. Rapid and frequent molecular testing is cited as a key component [Scarpetta et al., 2021] in effective strategies to identify active infections and prevent systemic outbreaks.

Serological tests look for an immunological response to the virus. A week or so after an individual is infected with SARS-CoV-2, the individual will start producing antibodies. At this point, a

serological test with perfect sensitivity will come back positive. This test provides evidence of past infection while the molecular test provides evidence of an *active* infection.

To better estimate SARS-CoV-2 immunity in a population, seroprevalence studies that generate a probabilistic population sample and perform serological tests on the sample can be collected. These studies are useful for disease surveillance. By June 2021, the CDC has conducted ten large-scale geographic serological surveys with three rounds. While population-based sampling strategies provide a more representative nationwide sample, they are very time intensive and expensive.

2.2. Publicly available data on COVID-19. The primary goal of this paper is to produce accurate estimates of the population-level active infection rates over time using *publicly available* viral testing data. Secondary goals include estimation of rates of change and the effective reproduction number which characterize disease trajectory. These quantities are fundamental to public health policy and provide critical information on the presence and transmission of SARS-CoV-2.

Coronavirus case-count data refers to the number of positive molecular tests performed on each day. Figure 1a plots the number of reported confirmed COVID-19 cases per day in the state of Indiana. Figure 1b plots the total number of COVID-19 molecular tests performed per day. Figure 1c plots the total number of COVID-19 related reported deaths per day. Public databases maintained by Johns Hopkins University and the New York Times provide accessible incoming county-level information of confirmed cases and deaths.

Public databases most often, however, only contain aggregate information. The Johns Hopkins dashboard, for example, provides demographic breakdown of case counts as well as the total confirmed cases and deaths by county. Aggregate time series of case count and deaths can also be extracted. Unfortunately, most dashboards do not provide demographic information on who requested a test nor on who tested positive for SARS-CoV-2 *over time*. Working closely with the State of Indiana, we were able to access COVID-19 total tests, positive tests, and related deaths per day broken out marginally by age, gender, ethnicity, and race [IDOH, 2021]. These granular datasets are now publicly available and motivate the proposed approach.

Remark 2 (Reporting Delays). *Figure 1 shows clear reduced testing and case count reporting on weekends compared to weekdays. Moreover, COVID-19 tests are reported on the day they were administered, while case counts are reported based on the date the positive test was reported to and*

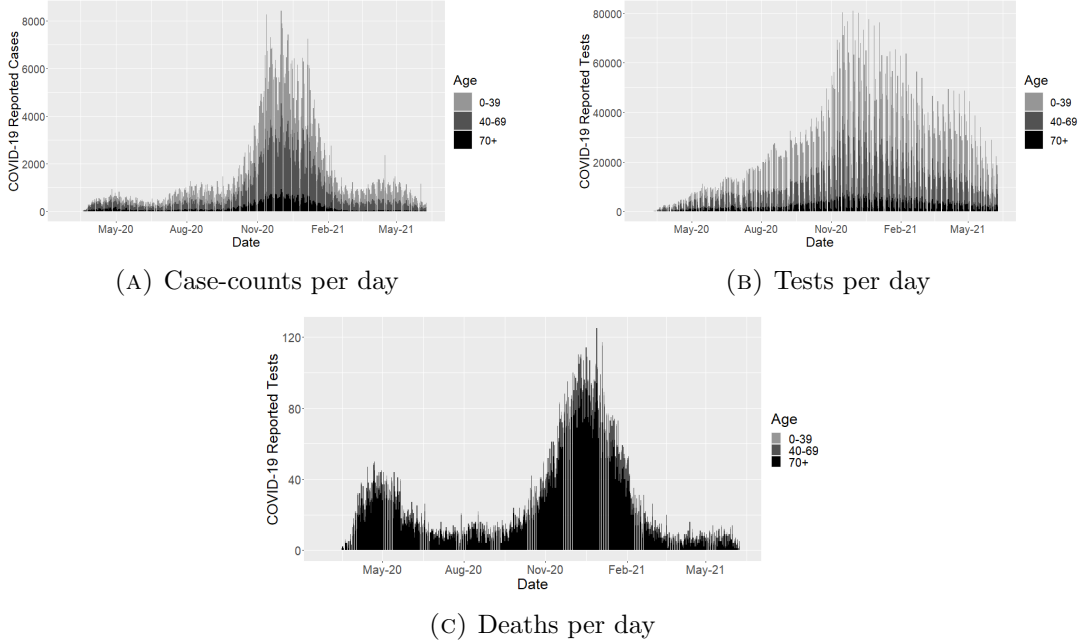


FIGURE 1. Indiana daily COVID-19 case count, testing, and death data by age strata

confirmed by the Indiana Department of Health system. To minimize the impact of reporting, testing and case-count data are aggregated at the weekly level for analysis.

Remark 3 (Public versus government datasets). *In this paper, we focus on publicly-available data, i.e., data that anyone can download directly from official government data portals such as the Indiana Data Hub (IDH). While the scientific community has contributed through independent COVID-19 observational and clinical studies, a significant component of public policy guidance has relied on testing and case count data, e.g., CDC and state guidelines based on test positivity rates and relative changes in the case counts over time. Addressing selection bias and measurement-error in these public datasets is imperative for better informed public policy debates.*

Note that Indiana’s COVID-19 response team has access to official government data which may not be publicly-available and is likely stored at the individual-level. Due to data privacy and legal concerns, some collected covariates may not be reported publicly and others are aggregated and reported marginally. While data analytic decisions discussed in Section 5 were made due to access of publicly-available data, the overall data analysis framework is designed to be a tool for health departments to assess the pandemic and guide responses, e.g., account for individual-level covariate

information, rather than publicly-reported strata-level information, that may include important covariates such as symptom status and recent COVID-19 contact.

2.2.1. Testing restrictions and public health policy in Indiana. Due to limited testing capacity, many US states instituted testing restrictions early on in the pandemic. Here, we reconstruct the testing restriction history for the state of Indiana. On March 6th, Indiana State Health Department of Health confirmed the first case of COVID-19 in Indiana. From early March 2020 until April 28th, 2020, only symptomatic essential workers and their households, symptomatic high risk individuals, and individuals who had returned recently from overseas travel were eligible. An individual was considered high risk if they were over the age of 65, diabetic, obese, pregnant, a member of a minority population at greater risk of severe illness, or had high blood pressure. On April 28th, 2020, the criteria expanded to include any symptomatic Indiana resident, people in close contact with those who had tested positive, and residents of congregant communities [Reports, 2020]. As of May 12th, 2020, testing expanded to include any high risk individual regardless of symptom status [Adams, 2020]. On June 15th, 2020, Indiana State Department of Health (ISDH) lifted all testing restrictions [Rudavsky, 2020]. Testing restrictions impact the propensity of an individual to receive a test and therefore, if COVID-19 positive, contribute to the case count. In this paper, testing restrictions are addressed by fitting time-varying testing propensities that depend on relevant covariate information.

On March 23rd, 2020, Indiana’s governor issued a *stay at home* order effective March 26th through April 5th. The order was extended until April 30th. On May 1st, 2020, a five-stage plan for gradual reopening was announced by Governor Holcomb [May, 2020]. Such policies target reduction in active infection rates. In this paper, Indiana’s public health policy is incorporated in our construction of epidemiological forecasts in Section 4.2.

2.3. Probabilistic samples in Indiana. Due to testing restrictions and other potential selection biases, publicly reported COVID-19 case count data may not be sufficient to understand active infection rates or the disease trajectory. Here, we discuss two random samples that provide auxiliary information and may help address selection bias.

2.3.1. *Random statewide testing.* Between April 25–29, 2020, Indiana conducted statewide random molecular testing of persons ages ≥ 12 years to assess prevalence of active infection to SARS-CoV-2 [Yiannoutsos et al., 2021]. A stratified random sampling design was conducted using Indiana’s 10 public health preparedness districts as sampling strata. 15,495 participants were contacted resulting in a final sample size of 3,658. Demographic data was collected (e.g., summary statistics on age, sex, and race) as well as data on whether they experienced any COVID-19 compatible symptoms during the past 2 weeks or had shared a household with someone who had a positive test result for SARS-CoV-2. During May 2–3, 2020, an additional non-random sample of 898 individuals was also collected. Table 1 summarizes the data.

		Total Tests (%)			IN Census	Positive Test Rate (%)	
		NonRandom	Random	CTIS		NonRandom	Random
Sex	Female	58.2	55.0	54.0	50.7	21.7 (11.2)	1.4
	Male	41.8	45.0	46.0	49.3	24.2 (12.4)	2.1
Age	< 40	39.4	28.0	36.2	52.7	29.7 (15.0)	1.7
	40 – 59	41.1	36.0	34.3	25.2	24.9 (12.5)	2.1
	≥ 60	19.5	36.0	29.5	22.1	6.7 (3.4)	0.9
Race	White	23.1	92.0	-	86.9	19.5 (9.6)	1.5
	Nonwhite	76.9	8.0	-	13.1	25.0 (12.3)	3.4
Fever	Yes	17.0	1.8	1.0	-	66.4 (32.1)	4.5
	No	83.0	98.2	99.0	-	15.6 (7.5)	1.3
Household + Case	Yes	10.8	1.4	1.8	-	46.1 (22.4)	29.4
	No	89.2	98.6	98.2	-	21.6 (10.4)	1.3
Prior + Test	Yes	6.1	1.4	-	-	39.2 (20.2)	24.4
	No	93.9	98.6	-	-	21.6 (11.1)	1.3

TABLE 1. Estimated total tests (%) and point prevalence of active infection with SARS-CoV-2 by demographics in Indiana [Yiannoutsos et al., 2021, Salomon et al., 2021]. NonRandom positive test rates in parentheses are adjusted rates to match the statewide rate of 11.7% on August 30th.

2.3.2. *Delphi’s COVID-19 Trends and Impact Survey.* Since April 2020, in collaboration with Facebook, the Delphi group at Carnegie Mellon University has conducted the COVID-19 Trends and Impact Survey (CTIS) to monitor the spread and impact of the COVID-19 pandemic in the United States. The survey is advertised through Facebook, who automatically select a random sample of its users to see the advertisement [Salomon et al., 2021]. Data collected includes basic demographic information and if the respondent has symptoms such as fever, coughing, shortness of breath, or loss of smell which are associated with COVID-19. The survey defines an individual

as displaying *COVID-like symptoms* if they exhibit a fever along with a cough, or shortness of breath, or difficulty breathing. Figure 2 displays smoothed estimates of the fraction of individuals who report COVID-like symptoms within the past 24-hours by age and gender. The Delphi’s COVID-19 Trends and Impact Survey (CTIS) is used as the main source of auxiliary information on time-varying characteristics of the population of Indiana, e.g., displaying COVID-like symptoms or in contact with COVID-19 positive individuals.

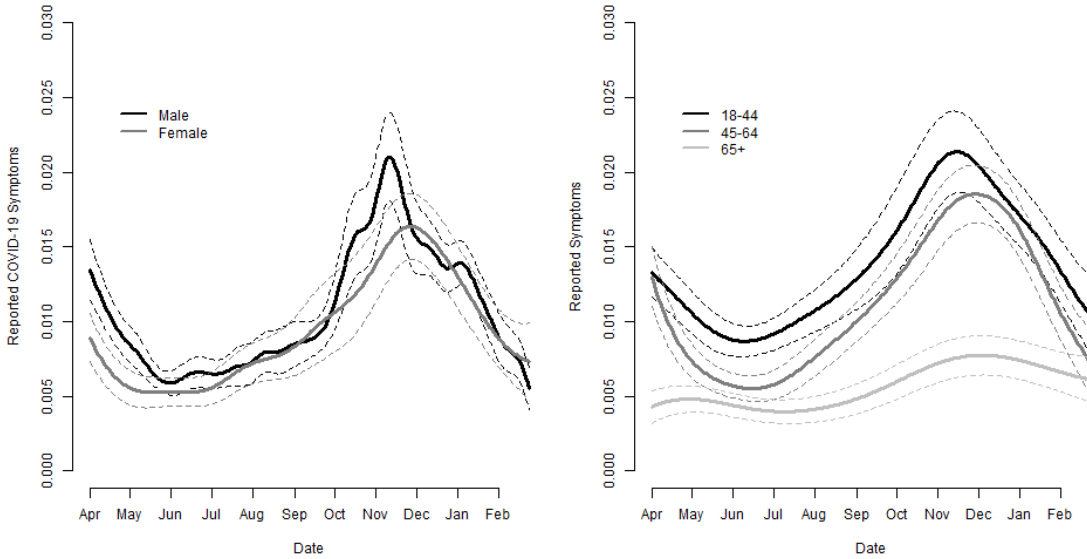


FIGURE 2. Rate of reported COVID-19 symptoms per strata. Daily rates were estimated using weighted method suggested by [Salomon et al., 2021] on each day separately and then smoothed over time using local-linear nonparametric regression.

3. ANALYSIS OF CASE-COUNT DATA

Let N denote the population size. At a given time, let Y_j denote COVID-19 status for the j th individual in the population, $j = 1, \dots, N$. Here, like in survey methodology [Cochran, 1977], we treat COVID-19 status as a fixed but unknown quantity of interest. For simplicity, we start by ignoring the dynamic nature of the outbreak and recoverability of individuals. We assume either individual j is COVID-19 positive and $Y_j = 1$ or is COVID-19 negative and $Y_j = 0$. We also let $I_j \in \{0, 1\}$ be an indicator that the individual was tested ($I_j = 1$) or not ($I_j = 0$).

To start, we assume the overall number of active COVID-19 cases and/or active infection rate (AIR) are of primary interest. That is, we are interested in either the population total $Y = \sum_{j=1}^N Y_j$ or the population average $\bar{Y} = Y/N$. Suppose that n tests are performed and we observe the

values $y_1, \dots, y_n \in \{0, 1\}$. Then a natural candidate for AIR is the proportion of positive tests $\bar{y} = \frac{1}{n} \sum_{i=1}^n y_i$ – commonly referred to as the test positivity rate – and a natural candidate for overall active cases is $N \times \bar{y}$. Under simple random sampling (SRS) or any other epsem² design, the above are unbiased estimators of the population-level quantities of interest. Under SRS, the variance of the estimator can be expressed as $\frac{1}{N-1} \times \frac{1-f}{f} \times \sigma_Y^2$ where $f = n/N$ is the sampling fraction and $\sigma_Y^2 = \frac{1}{N} \sum_{j=1}^N (Y_j - \bar{Y})^2 = \bar{Y}(1 - \bar{Y})$.

These random selection mechanisms are independent of the outcome of interest. When this is not the case, selection effects may cause bias. To better understand this issue, Meng [2018] recently provided the following intuitive and powerful statistical decomposition of the error between \bar{y} and the true proportion \bar{Y}

$$\bar{y}_n - \bar{Y} = \rho_{I,Y} \times \sqrt{\frac{1-f}{f}} \times \sigma_Y.$$

The first term represents *data quality*, the second *data quantity*, and the third *problem difficulty*. The term $\rho_{I,Y}$ is the empirical correlation between the population values $\{Y_j\}_{j=1}^N$ and the selection values $\{I_j\}_{j=1}^N$. Under simple random sampling, $E[\rho_{I,Y}] = 0$, so there is no bias.

3.1. Imperfect testing. Tests are imperfect. COVID-19 testing is no exception. Here we investigate the interplay between imperfect testing and selection bias. Researchers often assume measurement error leads to parameter attenuation. When paired with selection bias, however, the two sources become entangled, and resulting errors can be magnified, muted, or even switch signs.

Let P_j be an indicator of measurement error, equal to 1 when we incorrectly measure the binary outcome and 0 otherwise. We suppose this is a stochastic variable where $\text{pr}(P_j = 1 \mid Y_j = 1) =: FN$ is the false-negative rate and $\text{pr}(P_j = 1 \mid Y_j = 0) =: FP$ is the false-positive rate. If individual j is selected (i.e., $I_j = 1$) then the observed outcome can be written as $Y_j^* = Y_j(1 - P_j) + (1 - Y_j)P_j$. The attentive data analyst will recognize the estimator \bar{y}_n is now biased for simple random samples. In Appendix C.1.1, assuming sensitivity and specificity are known a priori, a novel iterative procedure is used to construct the estimator $\tilde{y}_n = (\bar{y}_n - FP)/(1 - (FP + FN))$, which is unbiased under simple random sampling (SRS); see Appendix C.2 for a discussion of the connection to model-based estimators. In the language of the epidemiology literature, the estimator \tilde{y}_n is the standard estimator for correcting for measurement error using false positive and negative rates that have been estimated

²equal probability of selection method

from a validation sample, where \bar{y}_n is the mis-measured average & \tilde{y}_n is the corrected average. To understand the impact of selection bias and imperfect testing, we derive the following statistical decomposition of the error between \tilde{y}_n and \bar{Y} :

$$(3.1) \quad \rho_{I,Y} \times \sqrt{\frac{1-f}{f}} \times \sigma_Y \times \underbrace{\left[1 - \Delta \times \frac{\bar{Y}}{1-\bar{Y}} \times \frac{FP(1-\bar{Y}) + FN \cdot \bar{Y}}{f_0(1-\bar{Y}) + f_1\bar{Y}} \right]}_{D_M} \times \frac{1}{1 - (FP + FN)},$$

where $f = n/N$ is the sampling fraction, f_1 and f_0 are sampling fractions for COVID-19 positive and negative individuals respectively, and $\Delta = f_1 - f_0$ is the sampling rate differential. See Appendix C.1.1 for the derivation. This extends work by Meng [2018] to account for imperfect testing. The first three terms continue to represent *data quality*, *data quantity*, and *problem difficulty* respectively. The new term D_M represents the *imperfect testing adjustment* which is a complex function of the sampling rate differential, the odds ratio, and the ratio of measurement error interaction with prevalence and sampling rates interaction with prevalence. For ease of comprehension, a notation glossary is provided in Section B in the supplementary materials.

Remark 4. *Note that test positivity is based on an underlying continuous cycle threshold and therefore not strictly binary. We focus on the interplay of measurement error and selection bias in the context of binary outcomes due to the dichotomous nature of the COVID-19 testing data. Also note that measurement error can lead to bias even in the absence of selection bias.*

Figure 3 shows that D_M , as a function of the relative frequency (f_1/f_0) and log odds ratio, can be both positive and negative as well as a range of magnitudes [Beesley et al., 2020, Beesley and Mukherjee, 2019, van Smeden et al., 2019]. Assuming no measurement error, $D_M = 1$ so the relation between estimation and selection bias is simple, e.g., if COVID-19 positive individuals were more likely to receive test then this implies upward bias in prevalence estimates. Under random testing (i.e., $f_0 = f_1$), $D_M = (1 - FP - FN)^{-1}$ so measurement error simply magnifies this error. When tests are imperfect and selection bias exists, this simple relationship no longer holds.

Comparing the mean-squared error (MSE) under a selection mechanism **I** with imperfect testing and SRS with perfect testing, we see that

$$\frac{E_{\mathbf{I}}[(\bar{y}_n - \bar{Y})^2]}{\sqrt{V_{SRS}(\bar{Y})}} = (N-1)E_{\mathbf{I}}[\rho_{I,Y}^2 D_M^2].$$

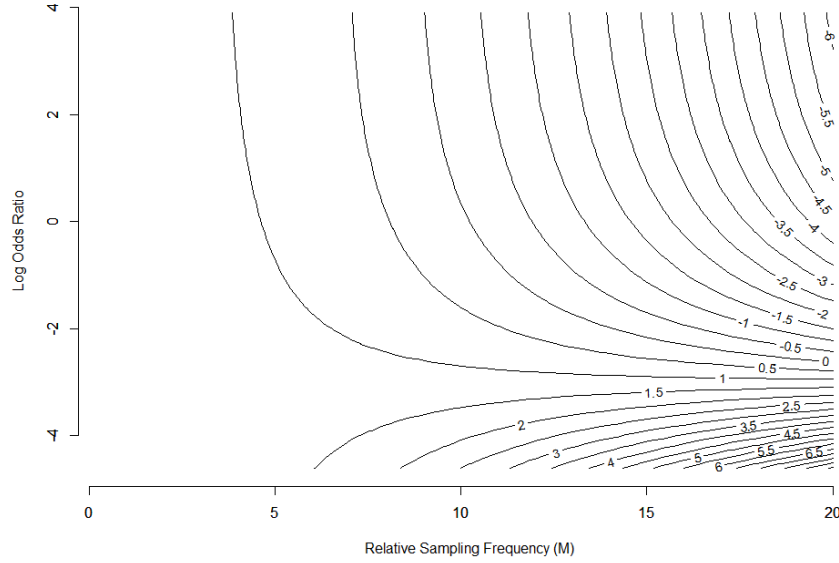


FIGURE 3. Imperfect testing adjustment (D_M) contour plot as a function of relative frequency f_1/f_0 (x-axis) and odds ratio (y-axis) for $FP = 0.024$ and $FN = 0.13$.

A key question is “What is the (effective) sample size from a SRS with perfect testing that would yield equivalent MSE to the current testing strategy?” In Appendix C.4, we show the effective sample size n_{eff} can be bounded by $\frac{f}{1-f} \times \frac{1}{E_I[\rho_{I,Y}^2 D_M^2]}$. Between April 25th to 29th 2020, Indiana performed 95,879 tests. Indiana’s population is roughly 6.732 million, so $f = 0.003$. The active infection rate was estimated to be 1.81% [Yiannoutsos et al., 2021] in this time interval. Recent studies have suggested 87% sensitivity [Arevalo-Rodriguez et al., 2020] and 97.6% specificity [Cohen et al., 2020] are reasonable measurement error rates for RT-PCR tests. Supposing COVID-19 positive individuals are 1.5 times more likely to get tested, then the effective sample size is 168. Recent proposals [Siddarth and Weyl, 2020] have argued for increased testing capacity, which may likely reduce the relative sampling rate. Even if the relative sampling rate drops to 1.2 and f increases to 0.01 then the effective sample size will increase to 1025. Thus the effective sample size even in optimistic scenarios is equivalent to a moderate random sample from the population. Moreover, increased testing capacity may alter false positive and negative rates due to changes in sample collection quality, e.g., a testing center switches from nasal swab to oropharyngeal swabs or saliva specimen to speed up data collection. Consider the case where f increasing from 0.003 to 0.01 and is associated with the false negative rate rising from 13% to 20%. Then the effective sample size is 863, representing a 5.1 factor increase rather than the expected 6.1 factor increase.

See Section C.7 in the Supplementary Materials for additional effective sample size calculations. Note that while [Meng, 2018] argues the relative error increases as a function of population size, calculations in our setting indicate this is not true when relative frequency f_1/f_0 is held fixed.

3.2. Regrettable rates: complex biases resulting from self-selection. The prior analysis demonstrates the potentially limited information regarding COVID-19 prevalence in observational case-count data. Analysts may claim that daily observed case-counts simply undercount daily total cases by a constant multiple over time (i.e., undercounting). If true then the ratio of case-counts at consecutive times may be a good estimate of the true change in prevalence, helping scientists understand the disease trajectory. We next demonstrate how selection bias and imperfect testing impact such estimates.

Let \bar{Y}_{t-1} and \bar{Y}_t denote the prevalence on two consecutive days and consider the estimator $r = \tilde{y}_t/\tilde{y}_{t-1}$. Using a second-order Taylor series approximation, the error between $\tilde{y}_t/\tilde{y}_{t-1}$ and \bar{Y}_t/\bar{Y}_{t-1} can be expressed approximately as

$$\begin{aligned} \frac{\bar{Y}_t}{\bar{Y}_{t-1}} \times & \left[\rho_{I_t, Y_t} D_{M_t} \sqrt{\frac{1-f_t}{f_t}} CV(Y_t) - \rho_{I_{t-1}, Y_{t-1}} D_{M_{t-1}} \sqrt{\frac{1-f_{t-1}}{f_{t-1}}} CV(Y_{t-1}) \right] \\ & \times \left[1 - \rho_{I_{t-1}, Y_{t-1}} D_{M_{t-1}} \sqrt{\frac{1-f_{t-1}}{f_{t-1}}} CV(Y_{t-1}) \right] \end{aligned}$$

where ρ_{I_j, Y_j} is the data quality, f_j is the sampling fraction, D_{M_j} is the measurement error adjustment, and $CV(Y_j) = \sigma_{Y_j}/\bar{Y}_j$ is the coefficient of variation on day j . See Appendix C.5 for the derivation. The error magnitude depends on the true rate \bar{Y}_t/\bar{Y}_{t-1} so a large decrease will have a small error relative to a large increase. The second term represents potential *cancellation* which can occur when data quality, sampling fraction, measurement error, and prevalence are constant across time.

Figure 4a displays the trajectory of the true ratio and the potential biased estimators under a susceptible-exposed-infected-recovered (SEIR) model [Pastor-Satorras and Vespignani, 2001, Newman, 2002, Parshani et al., 2010] for the epidemic dynamics, with state evolution given by

$$(3.2) \quad \begin{aligned} \frac{\partial s_t}{\partial t} &= -\beta s_t i_t; & \frac{\partial e_t}{\partial t} &= \beta s_t i_t - \sigma e_t; \\ \frac{\partial i_t}{\partial t} &= \sigma e_t - \gamma i_t; & \frac{\partial r_t}{\partial t} &= -\gamma i_t. \end{aligned}$$

where s_t, e_t, i_t and r_t are the fraction of susceptible, exposed, infected, and removed (recovered or deceased) individuals in the population at time t respectively. The SEIR model has been used extensively as a model for SARS-CoV-2 dynamics [Song et al., 2020]. In terms of bias, the rate is overestimated prior to the peak in the fraction infected and underestimated afterwards; the bias increases dramatically when the relative fraction exceeds 2. Such biases may impact policy making. Overestimation pre-peak may give policy makers more leverage in proposing aggressive actions to reduce prevalence. Underestimation post-peak puts pressure on policy makers to prematurely relax social distancing measures. Estimates at the peak time appear to have minimal bias.

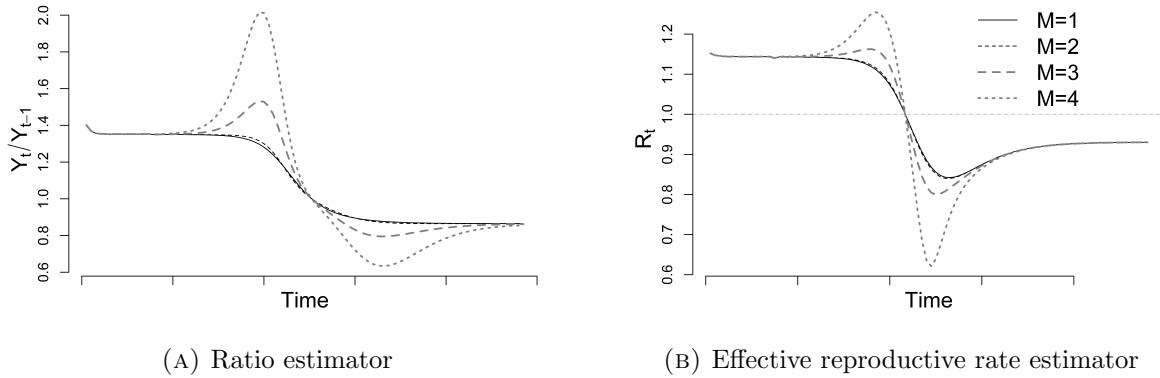


FIGURE 4. Potential bias in ratio and effective reproductive rate estimators under an SEIR model with $\beta = 1.2$, $\gamma = 0.15$, and $\sigma = 0.3$. Here, $f = 0.02$, $FP = 0.024$, $FN = 0.13$, and a range of relative sampling fractions $M = f_1/f_0$ are considered.

3.3. Estimation of effective reproduction number. Many epidemiologists argue that tracking the effective reproduction number is the only way to manage through the crisis [Leung, 2020]. Here, we study the instantaneous reproduction number [Cori et al., 2013, Fraser, 2007], denoted R_t , which is the average number of secondary cases that each infected individual would infect if the conditions remained as they were at time t . This is distinct from the case reproduction number, R_t^c , which is the average number of secondary cases that a case infected at time step t will eventually infect [Wallinga and Teunis, 2004]. The case reproduction number accounts for potential changes to contact rates and transmissibility, which include impact of control measures. The instantaneous reproduction number R_t is the only reproduction number easily estimated in real time, and therefore has been a key focal point in the COVID-19 pandemic.

Under a Poisson likelihood, a simple relation between the trajectory of new cases and the instantaneous reproduction number can be derived [Bettencourt and Ribeiro, 2008]. In particular, under an SIR model the number of case counts on day t , denoted K_t , is Poisson distributed with rate $K_{t-1} \exp(\gamma(R_t - 1))$ where $K_{t-1} = Y_{t-1} - Y_{t-2}$ is the number of new cases on day $t - 1$ and γ is the serial interval, which is approximately 7 days for COVID-19 [Sanche et al., 2020].

Heng and Althaus [2020] derive an approximate formula for the basic reproduction number under SEIR dynamics, which corresponds to the solution for the SIR model assuming an infectious period of $1/\gamma + 1/\sigma$ for $s_0 \approx 1$ and $i_0 \ll 1$. Using this connection, a moment-based estimator is given by

$$R_t \approx 1 + \left(\frac{1}{\gamma} + \frac{1}{\sigma} \right) \log \left(\frac{K_t}{K_{t-1}} \right).$$

This approximation ignores a term that is quadratic in the epidemic growth rate and inversely linear in $\sigma \times \gamma$; for realistic values of these quantities, however, the term is relatively negligible and therefore ignored. Of course, we do not observe K_t and K_{t-1} . Under SRS of new cases among those susceptible on day t , the natural estimator is $S_t \tilde{y}_t$. Unfortunately the number of susceptible individuals on day t is unknown. Here, we study the estimator $\hat{R}_t = 1 + \left(\frac{1}{\gamma} + \frac{1}{\sigma} \right) \log(\tilde{y}_t / \tilde{y}_{t-1})$. We can again express the statistical error of $\hat{R}_t - R_t$ in useful terms as follows

$$\begin{aligned} & \left(\frac{1}{\gamma} + \frac{1}{\sigma} \right) \log \left(1 + \left[\rho_{I_t, K_t} D_{M_t} \sqrt{\frac{1 - f_t}{f_t}} CV(K_t) - \rho_{I_{t-1}, K_{t-1}} D_{M_{t-1}} \sqrt{\frac{1 - f_{t-1}}{f_{t-1}}} CV(K_{t-1}) \right] \right. \\ & \quad \times \left. \left[1 - \rho_{I_{t-1}, K_{t-1}} D_{M_{t-1}} \sqrt{\frac{1 - f_{t-1}}{f_{t-1}}} CV(K_{t-1}) \right] \right) - \left(\frac{1}{\gamma} + \frac{1}{\sigma} \right) \log \left(\frac{S_t}{S_{t-1}} \right). \end{aligned}$$

This implies a similar trade-off as before but on the logarithmic scale. The error is no longer scaled by $\bar{Y}_t / \bar{Y}_{t-1}$ but by the serial interval and does not depend on prevalence but on the fraction of new cases out of those susceptible. This leads to differences in when the bias is most pronounced. Figure 4b displays the bias as a function of the relative sampling fraction ignoring the final term (i.e., $S_t / S_{t-1} \approx 1$). Section J in the supplementary materials presents an alternative estimator of the instantaneous effective reproductive number and shows similar bias Cori et al. [2013].

3.4. Rate comparisons. So far we have focused on understanding the limitations of using case-count data to understand population quantities of interest for a *single* population. Many are interested in cross-population comparisons to contrast the impact of countries' mitigation policies.

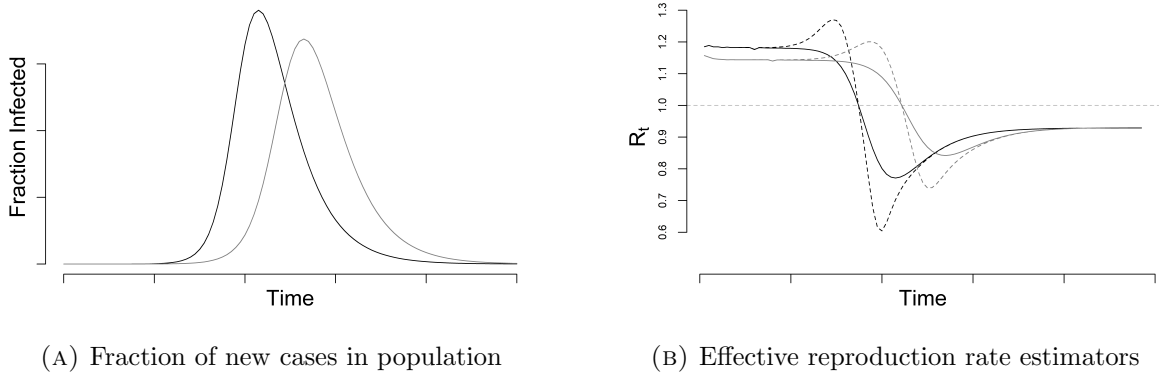


FIGURE 5. Left: fraction infected in two SEIR models with $\beta = 1.2$ and 0.9 respectively, $\sigma = 0.3$, and $\gamma = 0.15$ with same initial conditions. Right: comparison of \hat{R}_t across time with $FN = 0.30$, $FP = 0.024$, and $M = 4$.

Here, for simplicity, we focus on comparing the estimated effective reproductive rate. We assume the two time-series are aligned so that $t = 0$ is the time of first case in each population respectively.

Consider two countries (A and B) in which the peak occurs 2 weeks prior for country A than country B. Figure 5 presents such a comparison where each country's disease trajectory follows an SEIR model (A=black and B=grey). Figure 5b shows how biases interact in complex ways. At first, the difference is correctly estimated; then the gap is over-estimated as country A sees a rapid rise in cases; then the magnitude of over-estimation increases as country A sees declining case-count while country B sees rapidly increasing case-count; then country A's rate is correctly estimated while country B's rate is under-estimated as it sees declining case-count; finally, the gap disappears. While this may not always be the case, the analysis demonstrates how estimates can tell a more complex story than the truth (i.e., country A's peak is 2 weeks prior to country B's peak).

4. POTENTIAL IMPROVEMENTS TO PREVALENCE ESTIMATION

The prior section presented negative consequences of selection-bias and measurement error when estimating infection prevalence, rates of change, and the effective reproduction number from observed case-count data. In this section, we consider two directions to improve upon these estimators. The proposed methods and statistical error decompositions guide our recommendations in Section 6.

4.1. Selection propensity estimation. With non-probability samples, bias can be reduced by modelling the self-selection propensity and using inverse probability weighting (IPW) [Elliott and

Valliant, 2017] to adjust for selection bias. In the current context, however, one does not observe those who are not tested. To estimate selection propensities, auxiliary information is needed.

To see this mathematically, let X_j denote a vector of covariates for the j th individual in the population, $j = 1, \dots, N$. For simplicity, the dynamic nature of the outbreak and recoverability of individuals is ignored for now. Let I_j^{NR} denote the selection indicator for individual j in the population into the non-probability sample. Assume it is a Bernoulli random variable that depends only on these covariates, i.e., $P(I_j^{NR} = 1 \mid X_j = x) = \pi(x; \theta)$. Here, we focus on logistic regression models, i.e., $\pi(x; \theta) = \text{expit}(x^\top \theta)$. Maximum likelihood estimation follows by maximizing

$$(4.1) \quad \sum_{j=1}^N I_j^{NR} \log \left(\frac{\pi(X_j; \theta)}{1 - \pi(X_j; \theta)} \right) + \sum_{j=1}^N \log(1 - \pi(X_j; \theta)).$$

The first sum only involves individuals observed in the nonprobability sample. The second sum is over the entire population. Maximum likelihood estimation therefore requires knowledge of covariate information for every individual in the population. Typically, this is not possible. Here we present a method that uses auxiliary information obtained from probability samples.

4.1.1. Auxiliary information through probability samples. Here we assume access to a probability sample measuring the same set of covariates. Let I_j^R be an indicator that the individual was included in the probability sample and W_j^R be the probability of inclusion for the j th individual. Chen et al. [2019] use a probability sample to construct a design-unbiased estimator of the second term

$$(4.2) \quad \sum_{j=1}^N I_j^{NR} \log \left(\frac{\pi(X_j; \theta)}{1 - \pi(X_j; \theta)} \right) + \sum_{i=1}^N I_i^R W_i^R \log(1 - \pi(X_i; \theta)).$$

Expectation of 4.2 with respect to the sampling design yields (4.1). Solving (4.2) is done by iteratively re-weighted least squares (IRLS); see Section G and Section B in the supplementary materials for details and a notation glossary respectively.

Remark 5. *Weights built from selection propensities $\{\pi(x_i; \theta)\}_{i=1}^n$ are common practice in the epidemiology literature. Survey sampling and transportability weights require knowledge of the selection mechanism [Westreich et al., 2017, Cole and Stuart, 2010]. Here auxiliary information is required to estimate the selection propensities.*

4.1.2. *An IPW estimator and statistical error decomposition.* Given a selection propensity, define the inverse probability weight $w^{NR}(x) = \pi(x; \hat{\theta})^{-1}$. Then the IPW estimator adjusted for measurement error is given by

$$(4.3) \quad \bar{y}_n^* = \frac{1}{1 - FP - FN} \cdot \frac{\sum_{i=1}^n w^{NR}(x_i)(y_i - FP)}{\sum_{i=1}^n w^{NR}(x_i)} \stackrel{(2)}{=} \frac{1}{1 - FP - FN} \sum_{k=1}^K \frac{d_k w_k}{w} (\bar{y}_k - FP),$$

where equality (2) is under the assumption that x_i is a stratification variable with k indexing the strata, w_k is the weight and d_k is the number of samples in strata k , and $w = \sum_{k=1}^K d_k w_k$.

Let $I_j^{NR}(X_j) = I_j^{NR} \cdot w^{NR}(X_j)$ for $j = 1, \dots, N$. Then the error when comparing weighted estimator \bar{y}_n^* to the true prevalence \bar{Y} can be expressed as:

$$(4.4) \quad \rho_{I^{NR}(X), Y} \times \sqrt{\frac{1 - f + CV_W^2}{f}} \times \sigma_Y \times \underbrace{\left[1 - \tilde{\Delta} \times \frac{\bar{Y}}{1 - \bar{Y}} \times \frac{FP(1 - \bar{Y}) + FN \cdot \bar{Y}}{\tilde{f}_0(1 - \bar{Y}) + \tilde{f}_1 \bar{Y}} \right]}_{\tilde{D}_M} \times \frac{1}{1 - (FP + FN)}$$

where CV_W is the coefficient of variation (i.e., standard deviation/mean) of $w^{NR}(X_J)$ given $I_J = 1$, $\rho_{I^{NR}(X), Y}$ is the empirical correlation which here depends on covariate distribution, $\tilde{f}_k = E[w^{NR}(X_J)I_J | Y_J = k]$ for $k = 0, 1$, and $\tilde{\Delta} = \tilde{f}_1 - \tilde{f}_0$. See Appendix D for the derivation.

Comparing (4.4) to (3.1) shows that weighting impacts the estimation error in three ways. First, there is a negative impact on the data quantity component; taking the ratio of these quantities yields $\sqrt{1 + \frac{CV_W^2}{1-f}} \geq 1$. Hence, if the data quality does not increase (i.e., $|\rho_{I^{NR}(X), Y}| = |\rho_{I, Y}|$) then weighting increases the error magnitude. Second, the relative error increase depends on the fraction of population sampled f , implying that for large samples there is a larger potential increase in the error if the weights do not improve data quality. Third, the impact of measurement-error on data quality is changed when considering a weighted estimand. In particular, weighting may result in $\text{sgn}(\Delta) \neq \text{sgn}(\tilde{\Delta})$ which implies the impact of measurement-error may be in a different direction.

As demonstrated below in Lemma 4.1, if the propensity model is correctly specified then the $E[\rho_{I^{NR}(X), Y}] = 0$ and therefore $\rho_{I^{NR}(X), Y} = O(N^{-1})$; however, if the weights are not correctly specified then the data quality index is unlikely to inversely scale with population size. Similar to Meng [2018], if the data quality is not at the level of N^{-1} , then confidence intervals constructed from an IPW estimator are likely to put too much confidence in the sheer data size.

4.1.3. *Time-varying propensities.* Here we extend the IPW approach to the temporal setting to account for the dynamic nature of the outbreak by considering the joint likelihood

$$(4.5) \quad \sum_{t=1}^T \left[\sum_{j=1}^N I_{j,t}^{NR} \log \left(\frac{\pi_t(X_{j,t}; \theta)}{1 - \pi_t(X_{j,t}; \theta)} \right) + \sum_{j=1}^N \log (1 - \pi_t(X_{j,t}; \theta)) \right]$$

where $t = 1, \dots, T$ are the days when case-count data is reported, and $I_{j,t}^{NR}$ denotes self-selection into testing on day t , which is highly correlated with prior testing and results. For example, an individual who tests positive may be unlikely to seek testing in the subsequent few days/weeks. Moreover, an individual in a high prevalence area may be more likely to seek out testing. Here, we assume that the covariate vector $X_{j,t}$ contains all features of the past relevant for selection.

If sufficiently large random samples are collected at each time $t = 1, \dots, T$, then the pseudo-likelihood can be re-written as in (4.2) and propensities estimated separately per time point. Unfortunately, large probabilistic samples are not available at every time within a given region. To address this, here we consider a non-parametric kernel-based approach where the selection propensity at time t , denoted $\hat{\theta}_t$, maximizes the smoothed pseudo-likelihood

$$\sum_{t'=1}^T K_h(|t' - t|) \left[\sum_{j=1}^N I_{j,t'}^{NR} \log \left(\frac{\pi_t(X_{j,t'}; \theta)}{1 - \pi_t(X_{j,t'}; \theta)} \right) + \sum_{j=1}^N W_{j,t'}^R I_{j,t'}^R \log (1 - \pi_t(X_{j,t'}; \theta)) \right]$$

where K_h is a kernel function with tunable parameter h . Given $\pi(x; \hat{\theta}_t)$, the prevalence estimator $\bar{y}_{n,t}^*$ is given by 4.3 using case-count data observed on day t .

4.1.4. *Asymptotics.* Here we suppose there is a sequence of finite populations of size N_ν indexed by ν and that there are L_ν non-probability samples and probability samples of size n drawn at equally spaced times $\{t'_l\}_{l=1}^{L_\nu}$ over the study window $[0, T]$. Assuming correct selection model specification, then under the probability sample design and nonprobability sample propensities, Lemma 4.1 shows that the IPW estimator at a time $t \in \{t'_l\}$ is consistent as ν goes to infinity (i.e., $N_\nu, L_\nu \rightarrow \infty$) and calculates the estimator's variance. In Lemma 4.1, sensitivity/specificity are unknown and estimated using a pseudo-likelihood on two random samples whose sizes (denoted n_{FP} and n_{FN}) reflect uncertainty in these quantities. See Appendix F for additional details.

Lemma 4.1 (Variance of IPW estimator). The estimates $\hat{\mu}_t := \bar{y}_{n,t}^*$, $\hat{\pi}_{j,t}$, \hat{FP} , and \hat{FN} at a time $t \in \{t'_l\}$ are solutions to the following set of estimating equations

$$\Phi_n(\eta_t) = \begin{pmatrix} \frac{1}{N} \sum_{j=1}^N \frac{I_{j,t}^{NR} Y_{j,t} - FP - (1-FP-FN) \cdot \mu_t}{\pi_{j,t}} \\ \frac{1}{N \times \sum_{l=1}^L K_h(|t-t'_l|)} \sum_{l=1}^L K_h(|t-t'_l|) \left[\sum_{j=1}^N \frac{I_{j,t'_l}^{NR} X_{j,t'_l}}{\pi_{j,t'_l}} - \sum_{j=1}^N \frac{I_{j,t'_l}^R W_{j,t'_l}^R \pi_{j,t'_l} X_{j,t'_l}}{\pi_{j,t'_l}} \right] \\ \frac{1}{n_{FP}} \sum_{i=1}^{n_{FP}} \frac{Z_j}{FP} - \frac{1-Z_j}{1-FP} \\ \frac{1}{n_{FN}} \sum_{i=1}^{n_{FN}} \frac{\tilde{Z}_j}{FN} - \frac{1-\tilde{Z}_j}{1-FN} \end{pmatrix} = \mathbf{0}$$

where $\eta_t = (\mu_t, \pi_t, FP, FN)$. Under certain regularity assumptions (see Appendix F), we have $\bar{y}_{n,t}^* - \bar{Y}_t = O_p(\bar{n}^{-1/2})$ and $\text{var}(\hat{y}_{n,t}) = V_t^{(IPW)} + o(\bar{n}^{-1})$ where $\bar{n} = n \sum_{l=1}^L K_h(|t-t'_l|)$ and $V_t^{(IPW)}$ is the first diagonal element of $E[\phi_n(\eta_0)]^{-1} \text{Var}(\phi_n(\eta_0)) E[\phi_n(\eta_0)]^{-1}$ where $\phi_n = \frac{\partial \Phi(\eta)}{\partial \eta}$ with $E[\cdot]$ and $\text{Var}(\cdot)$ are under the joint randomization of propensity score and sampling designs.

4.2. Model-based estimation. Up to this point, the primary focus has been selection bias in coronavirus case-count data from a survey sampling perspective. Here, we consider compartmental model approaches from infectious disease epidemiology. Our primary objective is a model-based forecast of strata-level active infection rate \bar{y}_k . To do this, a probabilistic extension of a standard epidemiological state-space model – the susceptible, exposed, infected, and removed (recovered and death) model, or SEIR model – is presented. A probabilistic SIR model was originally proposed by Osthus et al. [2017] with only one-dimensional time series of infected proportions; this formulation was extended by Song et al. [2020] to model coronavirus case-counts.

Let s_t , e_t , i_t , and r_t denote the proportion of survivors, exposed, infected, and removed cases (i.e., including both recovered cases and deaths) at time t . The population-level SEIR dynamics are given by the set of differential equations in (3.2). Here, we consider covariate information that takes the form of a stratification variable with K strata. Based on these population-level dynamics, we can compute the number of *new infections* at time t , i.e., $I_t^{\text{new}} := -N \cdot (e_{t+1} - e_t + s_{t+1} - s_t)$ to denote the number of new infections on day t in the k th strata. The joint distribution of strata-specific new infections $\{I_{t,k}^{\text{new}}\}_{k=1}^K$ follows a multinomial distribution with

$$(I_{1,t}^{\text{new}}, \dots, I_{K,t}^{\text{new}}) \sim \text{Multinomial}(I_t^{\text{new}}, (p_{1,t}, \dots, p_{K,t})).$$

where $(\mathbf{p}_t)_{t=1}^T = ((p_{1,t}, \dots, p_{K,t}))_{t=1}^T$ are a sequence of parameters on the simplex, i.e., $\sum_{k=1}^K p_{k,t} = 1$.

Selection bias is addressed by analyzing COVID-19 death data rather than case counts. Let $D_{k,r}$ denote the number of individuals who pass away on day r from strata k . Then

$$D_{k,r} \mid p, \theta, \nu \sim \text{Poisson} \left(\sum_{t=1}^r \text{IFR}_k \cdot I_{k,t}^{\text{new}} \theta_{(r-t)} \right)$$

where IFR_k is the infection fatality rate for the k th strata and θ_j is a discrete-time distribution for time from infection to death. This extends prior analysis of death data Johndrow et al. [2020] by allowing the infection fatality rate to depend on a stratification variable, which is important as IFR depends heavily on age [Levin et al., 2020]. See Section 5.2 for discussion of parameter choices.

4.3. Doubly robust estimation. Rather than relying solely on IPW or epidemiological forecasts, here we combine forecasting and inverse-probability weighting by extending recent work by Chen et al. [2019] to account time-varying propensities and measurement-error. Let $\hat{\mu}(x)$ denote the posterior mean of the active infection rate individuals with covariate value x based on the SEIR model described in Section 4.2. In this context, the doubly-robust estimator is given by

$$\bar{y}_n^{(DR)} = \frac{1}{N} \sum_{j=1}^N \hat{\mu}(x_j) + \frac{1}{\sum_{j=1}^N I_j^{NR} w(x_j)} \sum_{j=1}^N I_j^{NR} w(x_j) \left(\frac{Y_j - FP}{1 - FP - FN} - \hat{\mu}(x_j) \right).$$

where $\hat{\mu}(x_j)$ is not corrected for measurement-error as it estimates true active infections. This estimator is called “doubly-robust” because it is consistent if either the model-based forecasts or the time-varying propensities are correctly specified. A statistical error decomposition can be derived

$$(4.6) \quad \begin{aligned} & \rho_{I^{NR}(X), Y - \mu(X)} \times \sqrt{\frac{1 - f + CV_W^2}{f}} \times \sigma_{Y - \mu(X)} \\ & \times \underbrace{\left[1 - \frac{\rho_{I^{NR}(X), Y} \sigma_Y}{\rho_{I^{NR}(X), Y - \mu(X)} \sigma_{Y - \mu(X)}} \times \tilde{\Delta} \times \frac{\bar{Y}}{1 - \bar{Y}} \times \frac{FP(1 - \bar{Y}) + FN \cdot \bar{Y}}{\tilde{f}_0(1 - \bar{Y}) + \tilde{f}_1 \bar{Y}} \right]}_{\tilde{D}_M}. \end{aligned}$$

See Appendix E for the derivation. If the model is adequate, then one may expect a reduction in the problem difficulty and (potentially) in the data quality components. Interestingly, the impact of measurement-error on data quality now depends on a relative comparison of the data quality and problem difficulty of the weighted estimator and the doubly-robust estimator.

Unfortunately, the first term of the doubly robust estimator cannot be computed as covariate information is not collected on the entire population. Here, we suppose the same asymptotic regime as in Section 4.1.4 and use the probability sample at the time $t \in \{t'_l\}$ to estimate this term:

$$\frac{1}{\sum_{j=1}^N I_{j,t}^R W_{j,t}^R} \sum_{j=1}^N I_{j,t}^R W_{j,t}^R \hat{\mu}_t(X_{j,t}) + \frac{1}{\sum_{j=1}^N I_{j,t}^{NR} w(X_{j,t})} \sum_{j=1}^N I_{j,t}^{NR} w(X_{j,t}) \left(\frac{Y_{j,t} - FP}{1 - FP - FN} - \hat{\mu}_t(X_{j,t}) \right).$$

Assuming correct selection propensity model specification, then under the probability sample design and nonprobability sample design, Lemma 4.2 shows that the doubly robust estimator is consistent and calculates the estimator's variance. See Appendix F for additional details.

Lemma 4.2 (Variance of doubly-robust estimator). The estimates $\mu_t := \bar{y}_{n,t}^*$ and $\hat{\pi}_{j,t}$ are solutions to the following set of estimating equations

$$\Phi_n(\eta_t) = \begin{pmatrix} \frac{1}{N} \left[\sum_{j=1}^N \frac{I_{j,t}^{NR}}{\pi_{j,t}} \left(\left(\frac{Y_{j,t} - FP}{1 - FP - FN} - \hat{\mu}_{j,t} \right) - \mu_t \right) + \frac{\sum_{l=1}^L K_h(|t - t'_l|) \sum_{j=1}^N I_{j,t'_l}^R W_{j,t'_l}^R \hat{\mu}_{j,t'_l}}{\sum_{l=1}^L K_h(|t - t'_l|) \sum_{j=1}^N I_{j,t'_l}^R W_{j,t'_l}^R} \right] \\ \frac{1}{N \times \sum_{l=1}^L K_h(|t - t'_l|)} \sum_{l=1}^L K_h(|t - t'_l|) \sum_{j=1}^N I_{j,t'_l}^{NR} X_{j,t'_l} - \frac{1}{N} \sum_{j=1}^N I_{j,t'}^R W_{j,t'}^R \pi_{j,t'} X_{j,t'} \\ \frac{1}{n_{FP}} \sum_{j=1}^{n_{FP}} \frac{Z_j}{FP} - \frac{1 - Z_j}{1 - FP} \\ \frac{1}{n_{FN}} \sum_{j=1}^{n_{FN}} \frac{\tilde{Z}_j}{FN} - \frac{1 - \tilde{Z}_j}{1 - FN} \end{pmatrix} = \mathbf{0}$$

where $\eta_t = (\mu_t, \pi_t, FP, FN)$. Under regularity assumptions (see Appendix F), we have $\bar{y}_{n,t}^* - \bar{Y}_t = O_p(\bar{n}^{-1/2})$ and $\text{var}(\hat{y}_{n,t}) = V_t^{(DR)} + o(\bar{n}^{-1})$ where $\bar{n} = n \sum_{l=1}^L K_h(|t - t_l|)$ and $V_t^{(DR)}$ is the first diagonal element of $E[\phi_n(\eta_0)]^{-1} \text{Var}(\Phi_n(\eta_0)) E[\phi_n(\eta_0)]^{-1}$ where $\phi_n = \frac{\partial \Phi(\eta)}{\partial \eta}$ with $E[\cdot]$ and $\text{Var}(\cdot)$ are under the joint randomization of propensity score and sampling designs.

5. COVID-19 ACTIVE INFECTION PREVALENCE IN INDIANA

We next consider estimation of the active infection rate in Indiana using unweighted, IPW, model-based, and doubly robust estimates. To start, we recap the data sources used in estimation:

- **Testing data:** The number of daily tests performed and number of daily positive tests are reported. These counts are broken out jointly by age, gender, and racial demographic information. Figure 1a and 1b plots daily COVID-19 positive cases and tests by age strata.
- **Random/Nonrandom statewide sample:** Table 1 summarizes data from a random sample from April 25–29th as well as a nonrandom sample obtained between May 2–3 in racial/ethnic

minority communities [Yiannoutsos et al., 2021]. The nonrandom sample is not a random subsample of the overall case-counts; however, this data provides important supplementary covariate information. To account for the nonrandom sample being from high risk areas, we adjust estimates to match the statewide positivity rate of 11.7% on August 30th. These adjusted rates are presented in parentheses in Table 1 along with the relevant covariate information.

- **Delphi’s COVID-19 Trends and Impact Survey:** From the daily symptom surveys completed as part of Delphi’s CTIS (see Section 2.3.2 for details), we extract survey responses for individuals who identify as living in Indiana. We collect age, sex, and demographic information as well as COVID-19 related symptoms, which Delphi defines as having (1) a fever and cough, (2) shortness of breath, *or* (3) difficulty breathing. Table 3 in Section H of the supplementary materials shows minimal bias with respect to symptom distributions when comparing to Indiana’s random sample to the CTIS data collected from April 25th to April 29th.
- **Death data:** Daily COVID-19 related deaths are observed by age, gender, and racial demographics. Figure 1c plots COVID-19 related deaths over time by age group. While most tests and positive cases are within the younger age strata, most deaths are within the 70+ age strata.

Remark 6. *We acknowledge several limitations with respect to representativeness of these samples. First, the random sample had significant missingness ($3,658/15,495 \approx 24\%$ response rate). See Yiannoutsos et al. [2021] for how the scientific team handled missing data in prevalence estimation. Second, the hit rate on randomly selected Facebook users is likely low and Facebook’s Indiana user population may differ from the Indiana population of interest. To address these concerns, the Delphi team provided respondent weights calculated by Facebook. See Barkay et al. [2020] for a description of the weights and corresponding methodology. Further adjustments are beyond the scope of this paper but are considered important future work. We urge health policy experts and government officials to assess these issues when applying this framework in their own work.*

5.1. Inverse-probability weighting approach. We start by using Table 1 to compute IPW weights for end of April, early May. The random sample is $n = 3,658$. IPW weights are computed per strata using Indiana Census and random survey data, and are allowed to depend on Gender, Age, Race, Fever, Positive Case in Household, and Prior Positive Test. The weight for the strata defined as Male, 40–59, White, has a Fever, no household cases, and no prior tests, for example, is

proportional to:

$$\frac{(0.493 \times 0.252 \times 0.869 \times 0.018 \times 0.986 \times 0.986)}{(0.418 \times 0.411 \times 0.231 \times 0.17 \times 0.892 \times 0.939)} \approx 0.334$$

Using the constructed weights and the adjusted strata-level prevalence estimates, the IPW estimate under no measurement-error is 7.7%, a decrease of four percentage points from the observed prevalence of 11.7%. We also make use of CTIS sample over that window of time to construct a second IPW estimate conditional on demographics and fever but ignoring the household and prior testing information, which under no measurement-error is 6.5%.

The Indiana study did not report sensitivity and specificity; therefore, we take the suggested measures from Arevalo-Rodriguez et al. [2020] which report 87% sensitivity is a reasonable estimates and Cohen et al. [2020] which report 97.6% specificity. This corresponds to a false negative rate of 13% and false positive rate of 2.4%, resulting in estimates of 6.2% and 4.9% using the random and CTIS samples respectively.

5.1.1. *Disease prevalence by April 2020.* Indiana’s population as of 2019 was 6.732 million. A total of 19,649 tests were administered in Indiana between April 25th to 29th. Subtracting off the 95,879 tests that had already performed yields a sampling fraction of $f = 2.96 \times 10^{-3}$. Here we consider estimation of data quality $E_{\mathbf{I}} [\rho_{INR(X),Y}]$. In Meng [2018], estimation relied on observing the true outcome (i.e., election vote totals). Here, we rely on Yiannoutsos et al. [2021] who use the random sample to estimate the true prevalence of active COVID-19 disease at 1.81% after accounting for non-response and measurement error. Our goal is to build sensitivity analyses to understand the amount of information in observational case-count data.

The unweighted estimate for the true prevalence of active COVID-19 disease between April 25th and April 29th is 11.7%. Assuming a false negative rate of 13% and false positive rate of 2.4%, the unweighted estimate is 11.0%, leading to an error of 9.2%. Using (3.1), an estimate of the relative sampling rate is

$$\rho D_M = \sqrt{\frac{f}{1-f}} \frac{0.092}{\sigma_Y} = 3.75 \times 10^{-2} \Rightarrow \Delta = 1.39 \times 10^{-2} \Rightarrow M = 6.1.$$

The IPW estimates for the prevalence of active COVID-19 disease between April 25th and April 29th adjusted for measurement-error are 6.2% and 4.9%, leading to errors 4.4% and 3.1% respectively.

Using (4.4), an estimate of the relative sampling rate is

$$\tilde{\rho}D_M = \sqrt{\frac{f}{1-f+CV_W^2}} \frac{0.044}{\sigma_Y} = 8.14 \times 10^{-3} \Rightarrow \tilde{\Delta} = 8.22 \times 10^{-3} \Rightarrow \tilde{M} = 3.9,$$

using the Indiana non-random sample. For the IPW estimate using CTIS data, $\tilde{M} = 3.3$. Therefore, bias is high using unweighted data and remains moderate using the weighted estimates.

A sensitivity analysis can be performed by considering the range of false negative/positive rates. Here, sensitivity ranges between 81% and 91% and specificity between 95% and 98.8% Katz et al. [2020]. This leads to a range for M of (5.60, 6.44) for the unweighted analysis, and (3.63, 4.07) and (3.10, 3.45) for the weighted analyses. Note that in calculating the sampling fraction f , we assumed individuals who tested recently are unlikely to test again in this time window. If we instead do not subtract off these tests, the sampling fraction is $f = 2.92 \times 10^{-3}$ and the above calculations change by a negligible amount.

5.1.2. Time-varying IPW estimator. The IPW analysis is next extended to the time-varying setting. To do so, we make use of the CTIS, hospitalization, and testing data. Recall the COVID-19 testing and positive case counts are known by age, gender, and racial demographics. Symptom status (e.g., fever, coughing, shortness of breath) and related covariate information (COVID-19 positive contact), however, are currently unavailable, which is likely due to data privacy considerations. As COVID-19 symptom status is likely to alter the testing propensity and likelihood of active infection, for illustrative purposes CTIS and hospitalization data are used in two ways to impute symptom status per strata. We outline the imputation methods below; see Section 6 for additional discussion.

In the first approach, we estimate two logistic regressions using weighted pseudo-likelihoods with the CTIS data. The first estimates the probability of contact with a COVID-19 positive individual given demographic and COVID-19 test status (positive or negative COVID-19 test). Figure 9a and 9b in Section H in the supplementary materials presents the estimated likelihood of contact with a COVID-19 positive individual given a negative and positive COVID-19 test in the past 24 hours respectively. The second estimates the probability of fever given demographic, COVID-19 test status, *and* whether the individual has had contact with a COVID-19 positive individual. Figure 10a and 10b in Section H in the supplementary materials presents the estimated likelihood of reporting a fever with a COVID-19 positive individual given a negative and positive COVID-19 test in the

past 24 hours respectively. We see that likelihood of fever varies greatly based on whether the individual also reported contact with a COVID-19 positive individual. Using these two models, mean imputation is used to calculate the number of positive and negative tests given demographic strata, fever status, and COVID-19 contact status. Inverse probability weights are computed based on the resulting dataset (termed IPW1).

In the second approach, we leverage hospitalization information. We first estimate the probability of fever given demographic and COVID-19 test status. When the COVID-19 test status is positive, the probability of fever is allowed to depend on whether the individual was hospitalized. Figure 12a and 12b in Section H in the supplementary materials presents the estimated likelihood of reporting a fever with a COVID-19 positive individual given a negative and positive COVID-19 test in the past 24 hours respectively. We see that hospitalization significantly increases the likelihood of fever as expected. We use these models and the case-to-hospitalization rates by demographic strata to perform mean imputation of the number of positive and negative tests given demographic strata, fever status, and COVID-19 contact status. The use of hospitalization data to estimate the probability of fever may be subject to survivor bias as well as biases driven by differential care. Inverse probability weights are then computed based on the resulting dataset (termed IPW2).

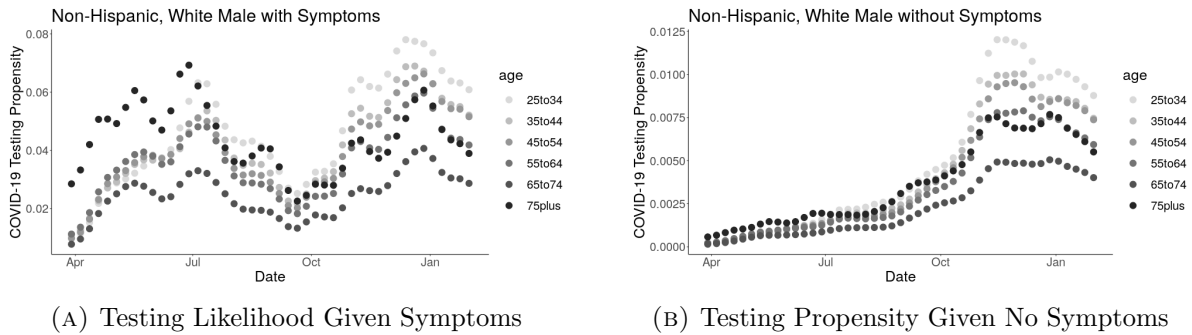


FIGURE 6. Testing Propensity across age strata and COVID-19 symptom status

Figure 6 presents the testing propensity for non-Hispanic, white males across age strata and fever status using the second approach. Note that the ratio of testing propensity within strata across fever status is time-varying, starting 50 times more likely in early April and dropping to ten times more likely by end of 2020. Similar plots for other strata and a discussion of their relative testing propensities can be found in Section H.2.1 of the supplementary materials.

5.2. Application of SEIR model. Here we consider the multinomial SEIR model using observed death data as presented in Figure 1c. The model, presented in Section 4.2, requires infection fatality rates to be specified per-strata. In this paper, similar to Johndrow et al. [2020], we specify fixed per-strata infection fatality rates. Based on published age-specific IFRs [Levin et al., 2020], IFR closely follows a log-linear relationship with age. Irons and Raftery [2021] uses Indiana’s random survey and death data to estimate a marginal IFR of 0.84%. Combining across published age-specific IFRs and anchoring our analysis to the estimated marginal IFR of 0.84% for Indiana, Table 2 presents the age-specific IFRs used in the analysis. The discrete-time distribution $\{\theta_j\}$ is a

Age Strata	0-40	50-59	60-69	70-79	80+
IFR	0.014%	0.120%	1.206%	3.815%	12.920%

TABLE 2. IFR by age-strata
 discretized version of a truncated normal distribution with mean 25, standard deviation 5, minimum value 0, and maximum value 44. This closely mirrors the distribution from Johndrow et al. [2020]. Strata for ages less than 40 are collapsed due to the limited number of COVID-19 related deaths in this age range. For similar reasons, the multinomial parameter \mathbf{p}_t is assumed to be constant in time with a symmetric Dirichlet prior.

Remark 7 (Sensitivity to IFR). *To account for potential misspecification of the marginal IFR, we perform the same analysis with a 10% increase and decrease in the marginal IFR under the log-linear model. Figure 19 in the supplementary materials presents the model-based and doubly robust estimates in these scenarios.*

The SEIR model in equation (3.2) is extended to allow for time-varying transmission rates β_t to account for public policy changes discussed in Section 2.2.1 over the time period considered. Here, we insert three change points (t_1, t_2, t_3) on March 23rd, June 15th, and October 1st of 2020 respectively. Given sensitivity to these choices, instead of considering a simple multiplicative structure, we allow for delayed implementation and slow change in the transmission rate by using weights:

$$\beta_t = \sum_{k=1}^3 \left(\beta_{k-1}(1 - w_t^{(k)}) + \beta_k w_t \right), \quad w_t^{(k)} = (1 + \exp(-\xi(t - t_k - \nu)))^{-1} \mathbf{1}[t \geq t_k]$$

where $(\beta_0, \beta_1, \beta_2, \beta_3)$ is the vector of transmission rate parameters, $\nu \geq 0$ is the potential delay, ξ is the rate of change, and $\mathbf{1}[\cdot]$ is an indicator function. Each weight $w_t^{(k)} = 0$ for $t < t_k$ and $w_t^{(k)} \rightarrow 1$ as $t \rightarrow \infty$. See Section I in the supplementary materials for details on prior specification.

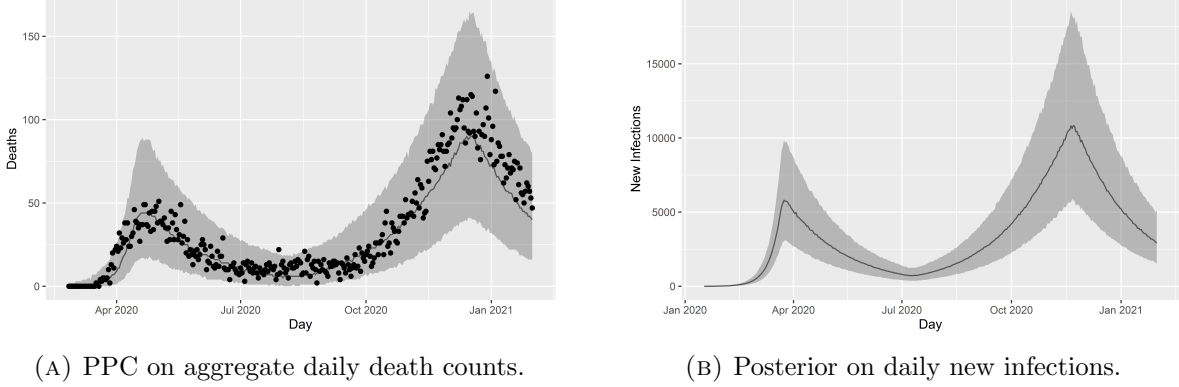


FIGURE 7. Posterior predictive check (PPC) on death counts and posterior distribution of infections.

To check model fit, a posterior predictive check on aggregate death counts was performed. Figure 7a shows the results which suggests chosen SEIR model fits the observed data well. Figure 7b presents the posterior distribution of daily new infections. As the active infection rate is defined as all infected individuals whose viral load has yet to fall below detectable levels by RT-PCR testing, to construct the active infection estimates we exponentially discount the number of newly infected individuals to estimate the number of these newly infected individuals who still have an active infection on future days. That is, the number of active infections on day t is given by $\sum_{s=0}^t I_t^{\text{new}} e^{-\lambda(t-s)}$. Strata-specific active infections are calculated similarly. In our analysis, the exponential discounting parameter is set to 20 days to match with prior evidence that “30% to 40% of people will still test positive at three weeks” [Brigman, 2020]. To compare with case count data, Figure 18 in the supplementary materials computes the cumulative undercount factor of observed case counts as compared to new infections. Posterior distributions for the age-specific new infections are used as part of the doubly-robust estimator of the active infection rate.

5.3. Time-varying prevalence estimates. Here, we construct active infection rate estimates using the unweighted, inverse-probability weighted, model-based, and doubly robust estimators. Figure 8 presents the results. The inverse-probability weighting methods does reduce bias compared to the unweighted estimates. Bias likely remains which we conjecture is due to the limited availability of symptom and other important covariate information to estimate strata-specific infection rates. This suggests better data collection in the future may strongly improve performance.

Model based estimates appear more reasonable. The estimate on the last week of April is 1.17% which is an underestimate when compared to the estimated prevalence using the stratified random sample of 1.81%. Caution is warranted when interpreting these estimates. Infection fatality rates are likely time-varying and may vary by other factors such as quality of healthcare and access to vaccines which were made available starting November 2020. Therefore, improvements could be made by using more accurate IFR estimates, but there is currently minimal publicly available data to do so. Moreover, the (thankfully) low number of deaths per strata make uncertainty in these estimates quite high. Finally, the doubly robust estimate appears similar to the IPW estimate, with the largest differences occurring in November and December 2020.

Figure 17 in the supplementary materials presents the confidence intervals per time point for the IPW2 estimator. The confidence interval length decreases substantially over time, reflecting the increased testing capacity over this window of time. Due to the number of surveys per week, there is minimal uncertainty in the parameter estimates. As the number of tests per week increases to over one hundred thousand, there is therefore minimal uncertainty in the active infection rate estimates. This points to the importance of the statistical decomposition (4.4) and the discussion in Section 4.1.2. Finally, given the reliance on a probabilistic sample with low response rate (see Remark 6), a sensitivity analysis showing the impact of a potential unmeasured confounder is presented in Section K of the supplementary materials.

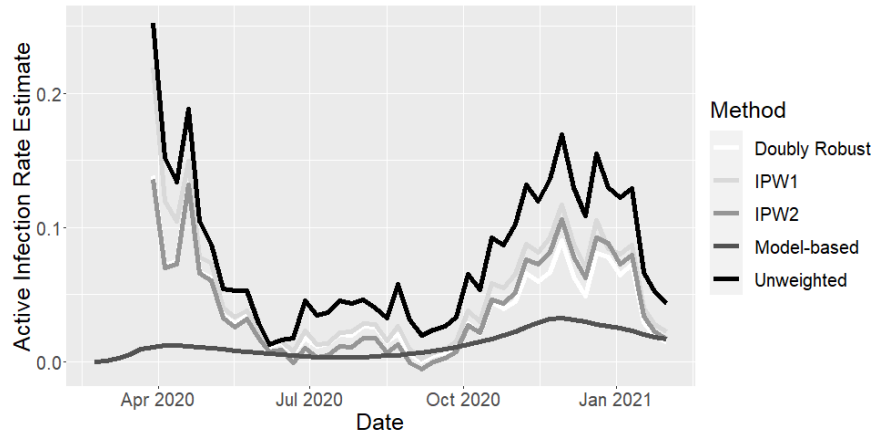


FIGURE 8. Time-varying active infection rate estimates based on unweighted, model-based, IPW and doubly robust methods.

6. DISCUSSION

There is nothing routine about COVID-19, including the corresponding statistical questions. The goal of this paper was to point out questionable statistical routines. Precision in reported case-count data gives the illusion of information when what is needed is quantification of uncertainty. Extensions of recent statistical error decompositions [Meng, 2018] demonstrate how selection bias leads data analysts to feel certain about incorrect conclusions. As case-count data is routinely used for public health policy making, we presented an inverse-probability weighting method and a doubly-robust estimation method that leverage auxiliary information collected through random samples to overcome these issues. We end with a brief discussion of important related topics.

Data quantity versus quality. Governments and policy makers often implicitly argue that increased testing capacity will alleviate selection bias. Without complete compliance, however, our understanding of future outbreaks may be plagued by self-selection bias, compounded by changing sensitivity and specificity rates of RT-PCR testing. Random testing removes these effect modifiers, giving governments more information to fight the disease. This paper emphasizes that data quantity is secondary to both data quality and methodological considerations to account for selection bias.

While we emphasize the importance of random sampling, we do not view it as a panacea. With access to *only* a non-probabilistic sample, we cannot address self-selection bias. Probability samples provide necessary auxiliary information to do so. Data analysts can then focus on statistical issues related to the random samples such as how to handle non-response bias. Covariates that the scientific team think are correlated with non-response (e.g., political affiliation, rural/urban location) should be collected as part of the random sampling protocol and corrected for in the data analysis. On the other hand, collecting covariate information that correlates with testing propensity (e.g., symptom status) in the non-probabilistic sample is insufficient.

Model-based solutions. A common argument is that the SEIR model can be extended to account for selection bias and measurement error directly; therefore, there is no need for auxiliary random sampling. Without strong assumptions on the selection mechanism, however, the estimates are often not identifiable. When an issue “cannot be resolved nonparametrically then it is usually dangerous to resolve it parametrically” [Cox and Hinkley, 1974]. Absent some type of random sampling, the

best route forward for all data analyses is careful associated sensitivity analyses and humility in data-driven conclusions. Irons and Raftery [2021], for example, use the Indiana seroprevalence random survey and to anchor their analysis; however, infrequent random surveys imply time-varying aspects such as the IFR may not be resolved by use of a single anchor.

Real-world implementation of the proposed method. The proposed methodology relied on access to two critical datasets: (1) COVID-19 testing, case, hospitalization, and death data by demographic strata and (2) CTIS data. Public access to (1) required submission of data requests to the state of Indiana. The author’s request was one of only five data requests to be approved by Indiana for public release. Most states do not release such granular data, making selection bias adjustments difficult. Coordinated, systematic data collection and reporting is critical. Lack of covariate information on individuals seeking COVID-19 tests is unacceptable. Random samples over time to supplement this data with auxiliary information is desperately needed. We acknowledge that this proposal will lead to data privacy concerns that will need to be addressed.

A valid criticism of the proposed approach is that recording covariates on every tested individual is time-consuming and costly. We argue that the list of relevant factors is of reasonable length. For example, symptom status and COVID-19 contact are clearly relevant factors in testing selection. Future work may consider how to include/exclude factors over time that are not significant to limit citizen reporting burden. Moreover, equation (4.2) presupposes covariate information is collected for all individuals in the nonprobability sample, which is often not feasible for state/local governments where rapid sample collection is prioritized. One can easily extend (4.2) by randomly sampling a subset of the nonprobability sample on which to collect the covariate information. This would balance goals of rapid testing and auxiliary data collection.

REFERENCES

- E.K. Accorsi, X. Qiu, E. Rumpler, L. Kennedy-Shaffer, R. Kahn, K. Joshi, E. Goldstein, M. Stensrud, R. Niehus, M. Cevik, and M. Lipsitch. How to detect and reduce potential sources of biases in studies of sars-cov-2 and covid-19. *Eur J Epidemiol*, 36:179–196, 2021.
- Dwight Adams. Coronavirus testing in indiana: Here’s who can get a test. <https://www.indystar.com/story/news/health/2020/05/12/coronavirus-testing-indiana-who-should-get-tested/3110592001/>, 2020.
- Ingrid Arevalo-Rodriguez, Diana Buitrago-Garcia, Daniel Simancas-Racines, Paula Zambrano-Achig, Rosa Del Campo, Agustin Ciapponi, Omar Sued, Laura Martinez-García, Anne W. Rutjes, Nicola Low, Patrick M. Bossuyt, Jose A. Perez-Molina, and Javier Zamora. False-negative results of initial rt-pcr assays for covid-19: A systematic review. *PLOS ONE*, 15(12):1–19, 12 2020. doi: 10.1371/journal.pone.0242958. URL <https://doi.org/10.1371/journal.pone.0242958>.
- N. Barkay, C. Cobb, R. Eilat, T. Galili, D. Haimovich, S. LaRocca, K. Morris, and T. Sarig. Weights and methodology brief for the covid-19 symptom survey by university of maryland and carnegie mellon university, in partnership with facebook, 2020.
- L. Beesley, L. Fritsche, and B. Mukherjee. An analytic framework for exploring sampling and observation process biases in genome and phenome-wide association studies using electronic health records. *Statistics in Medicine*, 2020.
- Lauren J Beesley and Bhramar Mukherjee. Statistical inference for association studies using electronic health records: handling both selection bias and outcome misclassification. *medRxiv*, 2019.
- LMA Bettencourt and RM Ribeiro. Real time bayesian estimation of the epidemic potential of emerging infectious diseases. *PLoS ONE*, 3(5):e2185, 2008.
- F. Breidt and J. Opsomer. Model-assisted survey estimation with modern prediction techniques. *Statistical Science*, 32(2):190–205, 2017.
- Lauren Brigman. How long does it take to test negative after testing positive for covid-19? <https://wlos.com/news/news-13-investigates/how-long-does-it-take-to-test-negative-after-testing-positive-for-covid-19>, 2020.
- Y. Chen, P. Li, and C. Wu. Doubly robust inference with nonprobability survey samples. *Journal of the American Statistical Association*, 2019.

- William G. Cochran. *Sampling Techniques, 3rd Edition*. John Wiley, 1977.
- Andrew N Cohen, Bruce Kessel, and Michael G Milgroom. Diagnosing covid-19 infection: the danger of over-reliance on positive test results. *medRxiv*, 2020. doi: 10.1101/2020.04.26.20080911. URL <https://www.medrxiv.org/content/early/2020/09/28/2020.04.26.20080911>.
- S. Cole and EA Stuart. Generalizing evidence from randomized clinical trials to target populations: The actg 320 trial. *Am J Epidemiol*, 172(1):107–15, 2010. doi: 10.1093/aje/kwq084.
- A Cori, NM Ferguson, C Fraser, and S Cauchemez. A new framework and software to estimate time-varying reproduction numbers during epidemics. *Am J Epidemiol*, 178(9):1505–1512, 2013.
- David R. Cox and David V. Hinkley. *Theoretical Statistics*. Chapman & Hall, London, England, 1974.
- E. Dong, H. Du, and L. Gardner. An interactive web-based dashboard to track covid-19 in real time. *Lancet Infect Dis*, 20:533–534, 2020.
- M. Elliott and R. Valliant. Inference for nonprobability samples. *Statistical Science*, 32(2):249–264, 2017.
- MP Fox, TL Lash, and LM Bodnar. Common misconceptions about validation studies. *Int J Epidemiol*, 49(4):1392–1396, 2020. doi: doi:10.1093/ije/dyaa090.
- C. Fraser. Estimating individual and household reproduction numbers in an emerging epidemic. *PLoS One*, 2(1):e758, 2007.
- G. Giordano, F. Blanchini, R. Bruno, P. Colaneri, A. Di Filippo, A. Di Matteo, and M. Colaneri. Modelling the covid-19 epidemic and implementation of population-wide interventions in italy. *Nature Medicine*, 2020.
- X. Hao, S. Cheng, D. Wu, T. Wu, X. Lin, and C. Wang. Reconstruction of the full transmission dynamics of covid-19 in wuhan. *Nature*, pages 420–424, 2020.
- Kevin Heng and Christian Althaus. The approximately universal shapes of epidemic curves in the susceptible-exposed-infectious-recovered (seir) model. *Scientific Reports*, 10(19365), 2020.
- D. G. Horvitz and D. J. Thompson. A generalization of sampling without replacement from a finite universe. *Journal of the American Statistical Association*, 47:663–685, 1952.
- IDOH. Covid-19 case demographics daily trend. <https://hub.mph.in.gov/dataset/covid-19-case-demographics-daily-trend/resource/c8a0ff06-7ff6-4932-b61e-a87ad2710797>, 2021. Accessed:

2021-06-15.

- IHME and Christopher JL Murray. Forecasting the impact of the first wave of the covid-19 pandemic on hospital demand and deaths for the usa and european economic area countries. *medRxiv*, 2020.
- Guido W. Imbens. Sensitivity to exogeneity assumptions in program evaluation. *American Economic Review*, 93(2):126–132, May 2003. doi: 10.1257/000282803321946921. URL <https://www.aeaweb.org/articles?id=10.1257/000282803321946921>.
- Nicholas J. Irons and Adrian E. Raftery. Estimating sars-cov-2 infections from deaths, confirmed cases, tests, and random surveys. *Proceedings of the National Academy of Sciences*, 118(31), 2021. ISSN 0027-8424. doi: 10.1073/pnas.2103272118. URL <https://www.pnas.org/content/118/31/e2103272118>.
- J. Johndrow, K. Lum, M. Gargiulo, and P. Ball. Estimating the number of sars-cov-2 infections and the impact of social distancing in the united states, 2020.
- R. Kahn, L. Kennedy-Shaffer, Y. Grad, J. Robins, and M. Lipsitch. Potential biases arising from epidemic dynamics in observational seroprotection studies. *American Journal of Epidemiology*, 192:328–335, 2021.
- AP Katz, FJ Civantos, Z Sargi, JM Leibowitz, E Nicolli, D Weed, A Moskovitz, A Civantos, Andrews D, O Martinez, and Thomas G. False-positive reverse transcriptase polymerase chain reaction screening for sars-cov-2 in the setting of urgent head and neck surgery and otolaryngologic emergencies during the pandemic: Clinical implications. *Head Neck*, 42(7):1621–1628, 2020.
- N. Keiding and T. A. Louis. Perils and potentials of self-selected entry to epidemiological studies and surveys. *Journal of the Royal Statistical Society: Series A (Statistics in Society)*, 179(2): 319–376, 2016.
- S Lauer, K Grantz, B Qifang, F Jones, Q Zheng, H Meredith, A Azman, N Reich, and J Lessler. The incubation period of coronavirus disease 2019 (covid-19) from publicly reported confirmed cases: Estimation and application. *Ann Intern Med.*, 172(9):577–582, 2020. doi: 10.7326/M20-0504.
- Gabriel Leung. Lockdown can’t last forever. here’s how to lift it. *New York Times*, 2020.
- Andrew T Levin, William P. Hanage, Nana Owusu-Boaitey, Kensington B. Cochran, Seamus P. Walsh, and Gideon Meyerowitz-Katz. Assessing the age specificity of infection fatality rates for covid-19: Systematic review, meta-analysis, and public policy implications. *medRxiv*, 2020. doi: 10.1101/2020.07.23.20160895. URL <https://www.medrxiv.org/content/early/2020/10/08/2020.07.23.20160895>.

- Ethan May. Each of indiana’s reopening stages, explained. <https://www.indystar.com/story/news/health/2020/05/01/when-indiana-reopen-here-phases-set-reopening/3067992001/>, 2020.
- Xiao-Li Meng. Statistical paradises and paradoxes in big data (i): Law of large populations, big data paradox, and the 2016 us presidential election. *Ann. Appl. Stat.*, 12(2):685–726, 2018.
- Michael J. Mina, Roy Parker, and Daniel B. Larremore. Rethinking covid-19 test sensitivity — a strategy for containment. *New England Journal of Medicine*, 383(22):e120, 2020. doi: 10.1056/NEJMp2025631. URL <https://doi.org/10.1056/NEJMp2025631>.
- MEJ Newman. Spread of epidemic disease on networks. *Phys. Rev. Lett.*, 66, 2002.
- D. Osthus, K. Hickmann, P. Caragea, D. Higdon, and S. Del Valle. Forecasting seasonal influenza with a state-space sir model. *Annals of Applied Statistics*, 11(1), 2017.
- R. Parshani, S. Carmi, and S. Havlin. Epidemic threshold for the sis model on random networks. *Phys. Rev. Lett.*, 104, 2010.
- R. Pastor-Satorras and A. Vespignani. Epidemic spreading in scale-free networks. *Phys. Rev. Lett.*, 86, 2001.
- Debashree Ray, Maxwell Salvatore, Rupam Bhattacharyya, Lili Wang, Shariq Mohammed, Soumik Purkayastha, Aritra Halder, Alexander Rix, Daniel Barker, Michael Kleinsasser, Yiwang Zhou, Peter Song, Debraj Bose, Mousumi Banerjee, Veerabhadran Baladandayuthapani, Parikshit Ghosh, and Bhramar Mukherjee. Predictions, role of interventions and effects of a historic national lockdown in india’s response to the covid-19 pandemic: data science call to arms. *medRxiv*, 2020.
- Staff Reports. Indiana opens up covid-19 testing to all hoosiers with symptoms. <https://www.wishtv.com/news/medical/indiana-opens-up-covid-19-testing-to-more-hoosiers/>, 2020.
- Shari Rudavsky. Want a coronavirus test? anyone can get one now, state says. here’s how. <https://www.indystar.com/story/news/health/2020/06/12/indiana-says-anyone-who-wants-coronavirus-test-can-get-one/3179151001/>, 2020.
- Joshua A. Salomon, Alex Reinhart, Alyssa Bilinski, Eu Jing Chua, Wichada La Motte-Kerr, Minttu M. Rönn, Marissa B. Reitsma, Katherine A. Morris, Sarah LaRocca, Tamer H. Farag, Frauke Kreuter, Roni Rosenfeld, and Ryan J. Tibshirani. The us covid-19 trends and impact survey: Continuous real-time measurement of covid-19 symptoms, risks, protective behaviors, testing, and vaccination. *Proceedings of the National Academy of Sciences*, 118(51):e2111454118,

2021. doi: 10.1073/pnas.2111454118. URL <https://www.pnas.org/doi/abs/10.1073/pnas.2111454118>.
- S Sanche, YT Lin, C Xu, E Romero-Severson, N Hengartner, and R Ke. High contagiousness and rapid spread of severe acute respiratory syndrome coronavirus 2. *Emerg Infect Dis.*, 2020.
- S Scarpetta, M Pearson, F Colombo, F Guanai, G Dedet, R Lopert, and M Wenz. Oecd policy responses to coronavirus (covid-19). <https://www.oecd.org/coronavirus/policy-responses/testing-for-covid-19-how-to-best-use-the-various-tests-c76df201/>, 2021. Accessed: 2021-06-15.
- D. Siddarth and E. Weyl. Why we must test millions a day. *COVID-19 Rapid Response Impact Initiative*, 2020.
- M. Smith, K. Yourish, S. Almukhtar, K. Collins, D. Ivory, and A. Harmon. Coronavirus in the us. *New York Times*, 2020.
- Peter X Song, Lili Wang, Yiwang Zhou, Jie He, Bin Zhu, Fei Wang, Lu Tang, and Marisa Eisenberg. An epidemiological forecast model and software assessing interventions on covid-19 epidemic in china. *medRxiv*, 2020. URL <https://www.medrxiv.org/content/early/2020/03/03/2020.02.29.20029421>.
- R. Valliant and J. Dever. Estimating propensity adjustments for volunteer web surveys. *Sociological Methods & Research*, 40(1):105 – 137, 2011.
- Maarten van Smeden, Timothy L Lash, and Rolf H H Groenwold. Reflection on modern methods: five myths about measurement error in epidemiological research. *International Journal of Epidemiology*, 49(1):338–347, 2019.
- Victor Veitch and Anisha Zaveri. Sense and sensitivity analysis: Simple post-hoc analysis of bias due to unobserved confounding. In H. Larochelle, M. Ranzato, R. Hadsell, M.F. Balcan, and H. Lin, editors, *Advances in Neural Information Processing Systems*, volume 33, pages 10999–11009. Curran Associates, Inc., 2020. URL <https://proceedings.neurips.cc/paper/2020/file/7d265aa7147bd3913fb84c7963a209d1-Paper.pdf>.
- J Wallinga and P Teunis. Different epidemic curves for severe acute respiratory syndrome reveal similar impacts of control measures. *Am J Epidemiol*, 160(6):509–516, 2004.
- Chaolong Wang, Li Liu, Xingjie Hao, Huan Guo, Qi Wang, Jiao Huang, Na He, Hongjie Yu, Xihong Lin, An Pan, Sheng Wei, and Tangchun Wu. Evolving epidemiology and impact of non-pharmaceutical interventions on the outbreak of coronavirus disease 2019 in wuhan, china. *medRxiv*, 2020.

- D. Westreich, J. Edwards, C. Lesko, S. Cole, and E. Stuart. Target validity and the hierarchy of study designs. *American Journal of Epidemiology*, 188(2), 2018.
- Daniel Westreich, Jessie K Edwards, Catherine R Lesko, Elizabeth Stuart, and Stephen R Cole. Transportability of Trial Results Using Inverse Odds of Sampling Weights. *American Journal of Epidemiology*, 186(8):1010–1014, 05 2017. ISSN 0002-9262. doi: 10.1093/aje/kwx164. URL <https://doi.org/10.1093/aje/kwx164>.
- Steven Woloshin, Neeraj Patel, and Aaron Kesselheim. False negative tests for sars-cov-2 infection – challenges and implications. *N Engl J Med*, 383(e38), 2020.
- Zifeng Yang, Zhiqi Zeng, Ke Wang, Sook-San Wong, Wenhua Liang, Mark Zanin, Peng Liu, Xudong Cao, Zhongqiang Gao, Zhitong Mai, Jingyi Liang, Xiaoqing Liu, Shiyue Li, Yimin Li, Feng Ye, Weijie Guan, Yifan Yang, Fei Li, Shengmei Luo, Yuqi Xie, Bin Liu, Zhoulang Wang, Shaobo Zhang, Yaonan Wang, Nanshan Zhong, and Jianxing He. Modified seir and ai prediction of the epidemics trend of covid-19 in china under public health interventions. *Journal of Thoracic Disease*, 12(3), 2020.
- Constantin T. Yiannoutsos, Paul K. Halverson, and Nir Menachemi. Bayesian estimation of sars-cov-2 prevalence in indiana by random testing. *Proceedings of the National Academy of Sciences*, 118(5), 2021. ISSN 0027-8424. doi: 10.1073/pnas.2013906118. URL <https://www.pnas.org/content/118/5/e2013906118>.
- Qingyuan Zhao, Nianqiao Ju, Sergio Bacallado, and Rajen D. Shah. BETS: The dangers of selection bias in early analyses of the coronavirus disease (COVID-19) pandemic. *The Annals of Applied Statistics*, 15(1):363 – 390, 2021. doi: 10.1214/20-AOAS1401. URL <https://doi.org/10.1214/20-AOAS1401>.

APPENDIX A. REPRODUCIBLE CODE

All relevant code can be found at <https://github.com/wdempsey/covid-umich>.

APPENDIX B. NOTATION GLOSSARY

Notation for Section 3 (non-temporal setting).

Y_j	Binary COVID-19 status of individual j in the population.
N	Population size
\bar{Y}	Population average, $\bar{Y} = N^{-1} \sum_{j=1}^N Y_j$
I_j	Selection indicator of individual j in the population into the sample
y_j	Binary COVID-19 status of sample individual $j = 1, \dots, n$.
\bar{y}_n	Sample average, $\bar{y}_n = n^{-1} \sum_{j=1}^N I_j Y_j = n^{-1} \sum_{j=1}^n y_j$
$\rho_{I,Y}$	<i>Data quality</i> , i.e., correlation between selection indicator and population outcome
f	<i>Data quantity</i> , i.e., sampling fraction $f = n/N$
σ_Y	<i>Problem Difficulty</i> , i.e., population variance $\sigma_Y^2 = (N)^{-1} \sum_{j=1}^N (Y_j - \bar{Y})^2$.
FP	False Positive Rate
FN	False Negative Rate
\tilde{y}_n	Sample average adjusted for false negative and positive rates, i.e., $\tilde{y}_n = (1 - FP - FN)^{-1}(\bar{y}_n - FP)$
f_0, f_1	Sampling fraction among COVID-19 negative and positive individuals respectively, i.e., $f_1 := \sum_{j=1}^N I_j Y_j / \sum_{j=1}^N Y_j$ and $f_0 := \sum_{j=1}^N I_j (1 - Y_j) / \sum_{j=1}^N (1 - Y_j)$.
Δ, M	Sampling rate differential on additive – $\Delta = f_1 - f_0$ – and multiplicative – $M = f_1/f_0$ – scales.

Notation for Section 4 (temporal setting).

$Y_{j,t}$	Binary COVID-19 status of individual j in the population at time t .
$I_{j,t}^{NR}$	Selection indicator of individual j in the population into the non-probability sample.
$X_{j,t}$	Feature vector for individual j in the population at time t that impact self-selection into the non-probability sample.
$I_{j,t}^R$	Selection indicator of individual j in the population into the probability sample.

- $W_{j,t}^R$ Weight of individual j in the population in the probability sample (i.e., inverse-probability of selection)
- $\pi(X_{j,t}; \theta)$ Self-selection propensity of individual j into the non-probability sample given feature vector $X_{j,t}$ and parameter θ .
- $w(X_{j,t})$ Weight of individual j in the population in the non-probability sample, i.e., $w(x) = 1/\pi(x; \theta)$.
- $\hat{\mu}(X_{j,t})$ Model-based estimate of the active infection rate at time t for individuals with feature vector $X_{j,t}$

APPENDIX C. TECHNICAL DETAILS

Recall that P_j is an indicator of measurement error, equal to 1 when we incorrectly measure the outcome and 0 when we observe the true outcome. We suppose this is a stochastic variable where $\text{pr}(P_j = 1 \mid Y_j = 1) =: FN$ is the false-negative rate and $\text{pr}(P_j = 1 \mid Y_j = 0) =: FP$ is the false-positive rate. If individual j is selected (i.e., $I_j = 1$) then the observed outcome can be written as $Y_j^* = Y_j(1 - P_j) + (1 - Y_j)P_j$.

C.1. Derivations for imperfect testing framework. We start by considering the empirical mean estimator under imperfect testing,

$$\bar{y}_n^* = \frac{\sum_{j=1}^N Y_j^* I_j}{\sum_{j=1}^N I_j} = \frac{\sum_{i=1}^N I_j Y_j^*}{\sum_{j=1}^N I_j} = \frac{\sum_{i=1}^N I_j [Y_j(1 - P_j) + (1 - Y_j)P_j]}{\sum_{j=1}^N I_j}$$

For any set of numbers $\{A_1, \dots, A_N\}$ we can view it as the support of a random variable A_J induced by the random index J defined on $\{1, \dots, N\}$. When J is uniformly distributed $E_J(A_J) = \sum_{j=1}^N A_j / N \equiv \bar{A}_N$. Then

$$\begin{aligned} \bar{y}_n^* - \bar{Y}_N &= \frac{E_J [I_J [Y_J(1 - P_J) + (1 - Y_J)P_J]]}{E_J[I_J]} - E_J[Y_J] \\ &= \frac{E_J [I_J P_J(1 - 2Y_J)]}{E_J[I_J]} + \left(\frac{E_J[I_J Y_J]}{E_J[I_J]} - \frac{E_J[Y_J]E_J[I_J]}{E_J[I_J]} \right) \end{aligned}$$

The term in parentheses can be re-written as

$$\begin{aligned} \frac{E_J[I_J Y_J] - E_J[Y_J] E_J[I_J]}{E_J[I_J]} &= \frac{E_J[I_J Y_J] - E_J[Y_J] E_J[I_J]}{\sqrt{V_J(I_J) V_J(Y_J)}} \frac{\sqrt{V_J(I_J)}}{E_J[I_J]} \times \sqrt{V_J(Y_J)} \\ &= \rho_{I,Y} \times \sqrt{\frac{(1-f)}{f}} \times \sigma_Y \end{aligned}$$

which agrees with Meng's (2019) decomposition. For the other term, first we define $Z_j := 1 - 2Y_j$.

Then $Z_j = 1$ if $Y_j = 0$ and $Z_j = -1$ if $Y_j = 1$. Then the term can be re-written as

$$\frac{E_J[I_J P_J (1 - 2Y_J)]}{E_J[I_J]} = \left(\frac{E_J[I_J P_J Z_J]}{E_J[I_J]} - \frac{E_J[P_J Z_J] E_J[I_J]}{E_J[I_J]} \right) + \frac{E_J[P_J Z_J] E_J[I_J]}{E_J[I_J]}$$

The term in parentheses can be re-expressed using the previous technique as:

$$\rho_{I,PZ} \times \sqrt{\frac{1-f}{f}} \times \sigma_{PZ}$$

where now the “data defect” and “problem difficulty” are with respect to PZ rather than Y . The final term is equal to

$$\begin{aligned} E_J[P_J Z_J] &= E_J[E_J[P_J Z_J \mid Y_J]] \\ &= \text{pr}(P = 1 \mid Y = 0)(1 - \bar{Y}) - \text{pr}(P = 1 \mid Y = 1)\bar{Y} \\ &= FP - (FP + FN) \cdot \bar{Y} \end{aligned}$$

Combining these yields:

$$\bar{y}_n^* - \bar{Y} = \sqrt{\frac{1-f}{f}} (\rho_{I,Y} \sigma_Y + \rho_{I,PZ} \sigma_{PZ}) + (FP - (FP + FN)\bar{Y})$$

C.1.1. Derivation of an estimator unbiased under SRS. We see the final term is given by $FP(1 - \bar{Y}) - FN\bar{Y}$ is the bias associated with using the unadjusted prevalence estimate \bar{y}_n^* . This motivates an adjusted estimate

$$\tilde{y}_n^{(0)} = \bar{y}_n^* - FP(1 - \bar{y}_n^*) + FN\bar{y}_n^* = \bar{y}_n^*(1 + FN + FP) - FP.$$

Now considering the error for the adjusted estimate, $\tilde{y}_n^{(0)} - \bar{Y}$, we have

$$\begin{aligned}
& \bar{y}_n^*(1 + FN + FP) - FP - \bar{Y} \\
&= (\bar{y}_n^* - \bar{Y}) + (FN + FP)\bar{y}_n^* - FP \\
&= \underbrace{\sqrt{\frac{1-f}{f}} [\rho_{I,Y}\sigma_Y + \rho_{I,PZ}\sigma_{PZ}]}_{\Psi} + (FN + FP)(\bar{y}_n^* - \bar{Y}) \\
&= \Psi + (FN + FP)\Psi + (FN + FP)(FP - (FP + FN)\bar{Y}).
\end{aligned}$$

The final term is a (smaller) bias term and so we propose another adjusted estimator $\tilde{y}_n^{(1)} = \tilde{y}_n^{(0)} + (FN + FP)((FN + FP)\bar{y}_n^* - FP)$, with associated error $\tilde{y}_n^{(1)} - \bar{Y}$ given by

$$\begin{aligned}
& (\tilde{y}_n^{(0)} - \bar{Y}) + (FN + FP)((FN + FP)\bar{y}_n^* - FP) \\
&= \Psi + (FN + FP)\Psi + (FN + FP)(FP - (FP + FN)\bar{Y}) + (FN + FP)((FP + FN)\bar{y}_n^* - FP) \\
&= \Psi + (FN + FP)\Psi + (FN + FP)^2\Psi + (FN + FP)^2(FP - (FP + FN)\bar{Y}).
\end{aligned}$$

This motivates recursively defining estimators $\tilde{y}_n^{(t)} = \tilde{y}_n^{(t-1)} + (FN + FP)((FN + FP)\tilde{y}_n - FP)$ for $t = 1, 2, \dots$ where $\tilde{y}_n^{(0)} = \bar{y}_n^*$. Then

$$\tilde{y}_n^{(t)} = \bar{y}_n^* \sum_{s=0}^{t+1} (FP + FN)^s - FP \sum_{s=0}^t (FP + FN)^s$$

and the associated error at iteration t given by

$$\Psi \sum_{s=0}^t (FN + FP)^s = \Psi \frac{1 - (FN + FP)^{t+1}}{1 - (FN + FP)}.$$

We can then get an estimator with no residual bias term by taking the limit as t goes to infinity; that is, define

$$\tilde{y}_n = \lim_{t \rightarrow \infty} \tilde{y}_n^{(t)} = \frac{\bar{y}_n^* - FP}{1 - (FN + FP)}.$$

Then the associated error $\tilde{y}_n - \bar{Y}$ can be expressed as $\frac{\Psi}{1 - (FN + FP)}$.

C.2. Model-based derivation of the estimator. The estimator \tilde{y} was derived as a limit of a process that removes the residual bias term at each step. Here we consider a model-based explanation. Let $\theta = \text{pr}(Y = 1)$ and $\phi = \text{pr}(\text{test is positive})$. Given a known false negative (FN) and false positive

(FP) rates, we have

$$\begin{aligned}\phi &= \theta \cdot (1 - FN) + (1 - \theta) \cdot FP = \theta(1 - FN - FP) + FP \\ \Rightarrow \theta &= \frac{\phi - FP}{1 - FN - FP}.\end{aligned}$$

Thus, the estimator \tilde{y} is also the appropriate estimator under a model-based approach. While the derivation here is more straightforward, the derivation in the prior section provides a simple formula for the associated error $\tilde{y}_n - \bar{Y}$ and gives a novel connection between the empirical estimator \bar{y}_n^* and the adjusted estimator \tilde{y}_n without reference to the model-based approach.

C.3. Further simplification. For the binary outcome Y , we have $\sigma_Y = \sqrt{\bar{Y}(1 - \bar{Y})}$. Moreover,

$$\begin{aligned}V_J(P_J Z_J) &= E_J[(P_J Z_J)^2] - E_J[P_J]E_J[Z_J] \\ &= E_J[P_J] - E_J[P_J](1 - 2\bar{Y}) = 2\bar{Y}E_J[P_J] \\ &= 2\bar{Y}(FP(1 - \bar{Y}) + FN\bar{Y}) \\ \Rightarrow \sigma_{PZ} &= \sqrt{2\bar{Y}(FP(1 - \bar{Y}) + FN \cdot \bar{Y})}\end{aligned}$$

Then the formula for the error is given by:

$$(C.1) \quad \sqrt{\frac{1-f}{f}} \left[\rho_{I,Y} \sqrt{\bar{Y}(1 - \bar{Y})} + \rho_{I,PZ} \sqrt{2\bar{Y}(FP(1 - \bar{Y}) + FN \cdot \bar{Y})} \right] \times \frac{1}{1 - (FN + FP)}$$

By definition, we have

$$\begin{aligned}\rho_{I,PZ} &= \frac{C(I, PZ)}{\sqrt{V(PZ)V(I)}} \\ &= \frac{C(I, PZ)}{\sqrt{V(Y)V(I)}} \sqrt{\frac{V(Y)}{V(PZ)}} \\ &= \rho_{I,Y} \frac{C(I, PZ)}{C(I, Y)} \sqrt{\frac{(1 - \bar{Y})}{2(FP(1 - \bar{Y}) + FN \cdot \bar{Y})}}\end{aligned}$$

$$\begin{aligned}
C(I, PZ) &= E[IPZ] - E[I]E[PZ] \\
&= [FPf_0 - (FPf_0 + FNf_1)\bar{Y}] - f[FP - (FP + FN)\bar{Y}] \\
&= -FP\Delta\bar{Y} + FP\bar{Y}^2\Delta - FN\bar{Y}^2\Delta \\
&= -\Delta\bar{Y}(FP \cdot (1 - \bar{Y}) + FN \cdot \bar{Y})
\end{aligned}$$

where $f = f_1\bar{Y} + f_0(1 - \bar{Y})$ so $f_0 - f = -\Delta\bar{Y}$ and $f_1 - f = \Delta(1 - \bar{Y})$.

$$\begin{aligned}
C(I, Y) &= E[IY] - f\bar{Y} \\
&= f_1\bar{Y} + f_0(1 - \bar{Y}) - f\bar{Y} \\
&= f_0(1 - \bar{Y}) + \Delta(1 - \bar{Y})\bar{Y} \\
&= (1 - \bar{Y})(f_0 + \Delta\bar{Y})
\end{aligned}$$

Combining yields

$$\begin{aligned}
\rho_{I,PZ} &= \rho_{I,Y} \times \frac{-\Delta\bar{Y}(FP \cdot (1 - \bar{Y}) + FN \cdot \bar{Y})}{(1 - \bar{Y})(f_0 + \Delta\bar{Y})} \times \sqrt{\frac{(1 - \bar{Y})}{2(FP(1 - \bar{Y}) + FN \cdot \bar{Y})}} \\
&= -\rho_{I,Y} \times \Delta \times \sqrt{\frac{\bar{Y}}{1 - \bar{Y}}} \frac{\sqrt{FP(1 - \bar{Y}) + FN \cdot \bar{Y}}}{f_0(1 - \bar{Y}) + f_1\bar{Y}} \times \sqrt{\frac{\bar{Y}}{2}}
\end{aligned}$$

We can then re-write $\rho_{I,Y}\sigma_Y + \rho_{I,PZ}\sigma_{PZ}$ as

$$\rho_{I,Y}\sigma_Y \left(1 - \Delta \times \frac{\bar{Y}}{1 - \bar{Y}} \times \frac{FP(1 - \bar{Y}) + FN \cdot \bar{Y}}{f_0(1 - \bar{Y}) + f_1\bar{Y}} \right).$$

Inserting into equation (C.1) yields the desired result.

C.4. Derivation of effective sample size. Let $S_Y^2 = (N - 1)^{-1} \sum_{j=1}^N (Y_j - \bar{Y})^2$ be the population variance as defined in survey sampling [Cochran, 1977]. Then $\sigma_Y^2 = (N - 1)/N \cdot S_Y^2$. Under SRS, the MSE is the variance as the estimate is unbiased and the variance is given by $(1 - f)/nS_Y^2$. Then

setting the MSE under general selection and SRS equal we have

$$\begin{aligned}
\underbrace{\frac{1-f}{f} \times E_{\mathbf{I}} [\rho_{I,Y}^2 \times D_M^2]}_{1/n_{eff}^*} \times \sigma_Y^2 &= \frac{1-f}{n_{eff}} S_Y^2 \\
\frac{1}{n_{eff}^*} \times \frac{N-1}{N} S_Y^2 &= \frac{1-f}{n_{eff}} S_Y^2 \\
\frac{1}{n_{eff}^*} &= \left(\frac{1}{n_{eff}} - \frac{1}{N} \right) \left(\frac{N}{N-1} \right) \\
\frac{1}{n_{eff}^*} \left[1 - \frac{1}{N} + \frac{n_{eff}^*}{N} \right] &= \frac{1}{n_{eff}} \\
n_{eff}^* \left[1 - \frac{1}{N} + \frac{n_{eff}^*}{N} \right]^{-1} &= n_{eff} \\
\frac{n_{eff}^*}{1 + (n_{eff}^* - 1)N^{-1}} &= n_{eff}
\end{aligned}$$

Then if $n_{eff}^* \geq 1$, we have that

$$n_{eff} \leq n_{eff}^* = \frac{f}{1-f} \times \frac{1}{E_{\mathbf{I}} [\rho_{I,Y}^2 \times D_M^2]}$$

C.5. Ratio estimator. Let $\mathbf{u} = (u_{t-1}, u_t) \in \mathbb{R}^2$ and $g(\mathbf{u}) = \frac{u_t}{u_{t-1}}$, i.e., a differentiable function $g : \mathbb{R}^2 \rightarrow \mathbb{R}$. Centering a Taylor series expansion of second-order around coordinates $(U_2, U_1) \in \mathbb{R}^2$ yields

$$\begin{aligned}
g(\mathbf{u}) &= g(U_{t-1}, U_t) - \frac{U_t}{U_{t-1}^2} (u_{t-1} - U_{t-1}) + \frac{1}{U_{t-1}} (u_t - U_t) \\
&\quad + \frac{1}{2} \left[\frac{2U_t}{U_{t-1}^3} (u_{t-1} - U_{t-1})^2 + 0 \times (u_t - U_t)^2 - 2 \times (u_{t-1} - U_{t-1})(u_t - U_t) \frac{1}{U_t^2} \right]
\end{aligned}$$

Plugging in $(\bar{y}_{t-1}, \bar{y}_t)$ for (u_{t-1}, u_t) and $(\bar{Y}_{t-1}, \bar{Y}_t)$ for (U_{t-1}, U_t) yields the $\frac{\bar{y}_t}{\bar{y}_{t-1}} - \frac{\bar{Y}_t}{\bar{Y}_{t-1}}$ is equal to

$$\begin{aligned}
&= -\frac{\bar{Y}_t}{\bar{Y}_{t-1}^2}(\bar{y}_{t-1} - \bar{Y}_{t-1}) + \frac{1}{\bar{Y}_{t-1}}(\bar{y}_t - \bar{Y}_t) \\
&\quad + \frac{\bar{Y}_t}{\bar{Y}_{t-1}^3}(\bar{y}_{t-1} - \bar{Y}_{t-1})^2 - (\bar{y}_{t-1} - \bar{Y}_{t-1})(\bar{y}_t - \bar{Y}_t)\frac{1}{\bar{Y}_{t-1}^2} \\
&= \frac{\bar{Y}_t}{\bar{Y}_{t-1}} \left[\rho_{I_t, Y_t} \sqrt{\frac{1-f_t}{f_t}} CV(Y_t) - \rho_{I_{t-1}, Y_{t-1}} \sqrt{\frac{1-f_{t-1}}{f_{t-1}}} CV(Y_{t-1}) \right. \\
&\quad \left. + \rho_{I_{t-1}, Y_{t-1}}^2 \frac{1-f_{t-1}}{f_{t-1}} CV^2(Y_{t-1}) - \rho_{I_{t-1}, Y_{t-1}} \sqrt{\frac{1-f_{t-1}}{f_{t-1}}} CV(Y_{t-1}) \times \rho_{I_t, Y_t} \sqrt{\frac{1-f_t}{f_t}} CV(Y_t) \right] \\
&= \frac{\bar{Y}_t}{\bar{Y}_{t-1}} \left[\rho_{I_t, Y_t} \sqrt{\frac{1-f_t}{f_t}} CV(Y_t) - \rho_{I_{t-1}, Y_{t-1}} \sqrt{\frac{1-f_{t-1}}{f_{t-1}}} CV(Y_{t-1}) \right] \left[1 - \rho_{I_{t-1}, Y_{t-1}} \sqrt{\frac{1-f_{t-1}}{f_{t-1}}} CV(Y_{t-1}) \right]
\end{aligned}$$

where the second equality is obtained by plugging in the statistical decomposition of the error for both time points and the coefficient of variation being defined as $CV(Y) := \sigma_Y/\mu_Y$. Under measurement error, the extra terms D_t and D_{t-1} can be inserted in the correct locations.

C.6. Estimation of effective reproduction number. Let

$$\delta_t := \left[\rho_{I_t, K_t} D_{M_t} \sqrt{\frac{1-f_t}{f_t}} CV(K_t) - \rho_{I_{t-1}, K_{t-1}} D_{M_{t-1}} \sqrt{\frac{1-f_t}{f_t}} CV(K_{t-1}) \right].$$

Then the previous sections derivation shows that the estimate of the number of new cases on day t is given by

$$\frac{S_t \cdot \bar{y}_t}{S_{t-1} \cdot \bar{y}_{t-1}} = \frac{K_t}{K_{t-1}} \left(1 + \delta_t \times \left[1 - \rho_{I_{t-1}, K_{t-1}} D_{M_{t-1}} \sqrt{\frac{1-f_t}{f_t}} CV(K_{t-1}) \right] \right)$$

Then setting $e_t = \delta_t \times [1 - \rho_{I_{t-1}, K_{t-1}} D_{M_{t-1}} \sqrt{\frac{1-f_t}{f_t}} CV(K_{t-1})]$, we have

$$\begin{aligned}
&\log \left(\frac{S_t \bar{y}_t}{S_{t-1} \bar{y}_{t-1}} \right) - \log \left(\frac{K_t}{K_{t-1}} \right) = \log(1 + e_t) \\
&\log \left(\frac{\bar{y}_t}{\bar{y}_{t-1}} \right) - \log \left(\frac{K_t}{K_{t-1}} \right) = 1 + e_t - \log \left(\frac{S_t}{S_{t-1}} \right) \\
&1 + \frac{1}{\gamma} \log \left(\frac{\bar{y}_t}{\bar{y}_{t-1}} \right) - \left[1 + \frac{1}{\gamma} \log \left(\frac{K_t}{K_{t-1}} \right) \right] = \frac{1}{\gamma} \left[\log(1 + e_t) - \log \left(\frac{S_t}{S_{t-1}} \right) \right] \\
&\Rightarrow \hat{R}_t - R_t = \frac{1}{\gamma} \left[\log(1 + e_t) - \log \left(\frac{S_t}{S_{t-1}} \right) \right]
\end{aligned}$$

C.7. Computing the effective sample size. For binary outcomes, we have

$$(C.2) \quad \rho_{I,Y} = \Delta \sqrt{\frac{\bar{Y}(1 - \bar{Y})}{f(1 - f)}}$$

where $\Delta = P_J(I_J = 1 \mid Y_J = 1) - P(I_J = 1 \mid Y_J = 0) = f_1 - f_0$. Suppose that $M = f_1/f_0$; then $f_0 = f/(\bar{Y} \cdot (M - 1) + 1)$. Using the upper bound $E_{\mathbf{I}}[\rho_{I,Y}^2] \leq E_{\mathbf{I}}[\rho_{I,Y}]^2$, we compute effective sample size under a range of prevalences \bar{y} , and relative sample rates M given $f = 0.003$ (i.e., current sampling fraction).

\bar{y}	M						
	1.05	1.15	1.25	1.35	1.45	1.55	1.65
0.01	40444	4503	1624	830	503	338	242
0.03	13787	1541	558	286	174	117	85
0.05	8463	950	345	178	109	73	53
0.07	6187	697	254	132	81	55	40
0.09	4928	557	204	106	65	44	32
0.11	4131	469	173	90	56	38	28

We also present the same plot under $FP = 0.024$ and $FN = 0.13$ to show the impact of measurement error on effective sample size.

	M						
	1.05	1.15	1.25	1.35	1.45	1.55	1.65
0.01	29019	3247	1177	605	368	248	179
0.03	9894	1112	405	209	128	87	63
0.05	6075	686	251	130	80	54	39
0.07	4442	504	185	96	59	41	30
0.09	3539	403	149	78	48	33	24
0.11	2967	339	126	66	41	28	21

For binary outcomes, we have

$$(C.3) \quad \rho_{\tilde{I}(X),Y} = \tilde{\Delta} \sqrt{\frac{\bar{Y}(1 - \bar{Y})}{f(1 - f)E(W_J \mid I_J = 1)^2 + f\text{Var}(W_J \mid I_J = 1)}}$$

APPENDIX D. IPW STATISTICAL ERROR DECOMPOSITION DERIVATION

We start by considering the empirical weighted mean estimator under imperfect testing,

$$\bar{y}_n^* = \frac{\sum_{j=1}^N W_j Y_j^* I_j}{\sum_{j=1}^N W_j I_j} = \frac{\sum_{i=1}^N I_j W_j Y_j^*}{\sum_{j=1}^N I_j} = \frac{\sum_{i=1}^N I_j [Y_j(1 - P_j) + (1 - Y_j)P_j]}{\sum_{j=1}^N I_j}$$

Then

$$\begin{aligned}\bar{y}_n^* - \bar{Y}_N &= \frac{E_J[I_J W_J [Y_J(1 - P_J) + (1 - Y_J)P_J]]}{E_J[I_J W_J]} - E_J[Y_J] \\ &= \frac{E_J[I_J W_J P_J(1 - 2Y_J)]}{E_J[I_J W_J]} + \left(\frac{E_J[I_J W_J Y_J]}{E_J[I_J W_J]} - \frac{E_J[Y_J]E_J[I_J W_J]}{E_J[I_J W_J]} \right)\end{aligned}$$

The term in parentheses can be re-written as

$$\begin{aligned}\frac{E_J[I_J W_J Y_J] - E_J[Y_J]E_J[I_J W_J]}{E_J[I_J W_J]} &= \frac{E_J[I_J W_J Y_J] - E_J[Y_J]E_J[I_J W_J]}{\sqrt{V_J(I_J W_J)V_J(Y_J)}} \frac{\sqrt{V_J(I_J W_J)}}{E_J[I_J]} \times \sqrt{V_J(Y_J)} \\ &= \rho_{\bar{I}(X), Y} \times \frac{\sqrt{V_J(I_J W_J)}}{E_J[I_J]} \times \sigma_Y\end{aligned}$$

Then

$$\begin{aligned}E_J(I_J W_J) &= P(I_J = 1)E_J[W_J | I_J = 1] = f \times E_J[W_J | I_J = 1] \\ V_J(I_J W_J) &= E[I_J W_J^2] - E[I_J W_J]^2 \\ &= f \cdot (E[W_J^2 | I_J = 1] - fE[W_J | I_J = 1]^2) \\ &= f \cdot (E[W_J^2 | I_J = 1] \pm E[W_J | I_J = 1]^2 - fE[W_J | I_J = 1]^2) \\ &= f \cdot (V(W_J | I_J = 1) + E[W_J | I_J = 1]^2(1 - f))\end{aligned}$$

Taking the ratio:

$$\sqrt{\frac{f \cdot (V(W_J | I_J = 1) + E[W_J | I_J = 1]^2(1 - f))}{f^2 E_J[W_J | I_J = 1]^2}} = \sqrt{\frac{1 - f + CV(W)^2}{f}}$$

which agrees with Meng's (2019) decomposition of weighted outcome. For the other term, first we define $Z_j := 1 - 2Y_j$. Then $Z_j = 1$ if $Y_j = 0$ and $Z_j = -1$ if $Y_j = 1$. Then the term can be re-written as

$$\frac{E_J[I_J W_J P_J(1 - 2Y_J)]}{E_J[I_J W_J]} = \left(\frac{E_J[I_J W_J P_J Z_J]}{E_J[I_J W_J]} - \frac{E_J[P_J Z_J] E_J[I_J W_J]}{E_J[I_J W_J]} \right) + \frac{E_J[P_J Z_J] E_J[I_J W_J]}{E_J[I_J W_J]}$$

The term in parentheses can be re-expressed using the previous technique as:

$$\rho_{\bar{I}, PZ} \times \sqrt{\frac{1 - f + CV(W)^2}{f}} \times \sigma_{PZ}$$

where now the “data defect” and “problem difficulty” are with respect to PZ rather than Y . The final term is equal to

$$\begin{aligned} E_J[P_J Z_J] &= E_J[E_J[P_J Z_J \mid Y_J]] \\ &= \text{pr}(P = 1 \mid Y = 0)(1 - \bar{Y}) - \text{pr}(P = 1 \mid Y = 1)\bar{Y} \\ &= FP - (FP + FN) \cdot \bar{Y} \end{aligned}$$

Combining these yields:

$$\bar{y}_n^* - \bar{Y} = \sqrt{\frac{1 - f + CV(W)^2}{f}} \left(\rho_{\tilde{I}(X), Y} \sigma_Y + \rho_{\tilde{I}(X), PZ} \sigma_{PZ} \right) + (FP - (FP + FN)\bar{Y})$$

By previous arguments, we have

$$\rho_{\tilde{I}(X), PZ} = \rho_{\tilde{I}(X), Y} \times \frac{C(\tilde{I}(X), PZ)}{C(\tilde{I}(X), Y)} \sqrt{\frac{1 - \bar{Y}}{2(FP(1 - \bar{Y}) + FN\bar{Y})}}$$

Then

$$\begin{aligned} C(IW, PZ) &= E[IWPZ] - E[IW]E[PZ] \\ &= [FP\tilde{f}_0 - (FP\tilde{f}_0 + FN\tilde{f}_1)\bar{Y}] - \tilde{f} \cdot (FP - (FP + FN)\bar{Y}) \\ &= -FP\tilde{\Delta}\bar{Y} + FP\bar{Y}^2\Delta - FN\bar{Y}^2\Delta \\ &= -\tilde{\Delta}\bar{Y}(FP \cdot (1 - \bar{Y}) + FN \cdot \bar{Y}) \end{aligned}$$

where $\tilde{f}_i = E[I_J W_J \mid Y_J = i]$ for $i \in \{0, 1\}$ and $f = \tilde{f}_1\bar{Y} + \tilde{f}_0(1 - \bar{Y})$. Moreover,

$$\begin{aligned} C(\tilde{I}, Y) &= E[IWY] - \tilde{f}\bar{Y} \\ &= \tilde{f}_1\bar{Y} + \tilde{f}_0(1 - \bar{Y}) - \tilde{f}\bar{Y} \\ &= \tilde{f}_0(1 - \bar{Y}) + \tilde{\Delta}(1 - \bar{Y})\bar{Y} \\ &= (1 - \bar{Y})(\tilde{f}_0 + \tilde{\Delta}\bar{Y}) \end{aligned}$$

Combining yields

$$\begin{aligned}\rho_{\tilde{I}(X),PZ} &= \rho_{\tilde{I}(X),Y} \times \frac{-\tilde{\Delta}\tilde{Y}(FP \cdot (1 - \tilde{Y}) + FN \cdot \tilde{Y})}{(1 - \tilde{Y})(\tilde{f}_0 + \tilde{\Delta}\tilde{Y})} \times \sqrt{\frac{(1 - \tilde{Y})}{2(FP(1 - \tilde{Y}) + FN \cdot \tilde{Y})}} \\ &= -\rho_{\tilde{I}(X),Y} \times \Delta \times \sqrt{\frac{\tilde{Y}}{1 - \tilde{Y}}} \frac{\sqrt{FP(1 - \tilde{Y}) + FN \cdot \tilde{Y}}}{\tilde{f}_0(1 - \tilde{Y}) + \tilde{f}_1\tilde{Y}} \times \sqrt{\frac{\tilde{Y}}{2}}\end{aligned}$$

We can then re-write $\rho_{\tilde{I}(X),Y}\sigma_Y + \rho_{\tilde{I}(X),PZ}\sigma_{PZ}$ as

$$\rho_{\tilde{I}(X),Y}\sigma_Y \left(1 - \tilde{\Delta} \times \frac{\tilde{Y}}{1 - \tilde{Y}} \times \frac{FP(1 - \tilde{Y}) + FN \cdot \tilde{Y}}{\tilde{f}_0(1 - \tilde{Y}) + \tilde{f}_1\tilde{Y}}\right).$$

Thus yielding the desired result.

APPENDIX E. DOUBLY ROBUST STATISTICAL ERROR DECOMPOSITION DERIVATION

We start by considering the empirical weighted mean estimator under imperfect testing,

$$\begin{aligned}&\frac{1}{N} \sum_{j=1}^N \mu(X_j) - \frac{\sum_{j=1}^N I_j W_j \mu(X_j)}{\sum_{j=1}^N I_j W_j} + \frac{\sum_{j=1}^N I_j W_j Y_j^*}{\sum_{j=1}^N I_j W_j} \\ &= \frac{\sum_{j=1}^N I_j W_j ([Y_j(1 - P_j) + (1 - Y_j)P_j] - \mu(X_j))}{\sum_{j=1}^N I_j W_j} + \frac{1}{N} \sum_{j=1}^N \mu(X_j)\end{aligned}$$

Then

$$\begin{aligned}&\frac{E_J [I_J W_J ([Y_J(1 - P_J) + (1 - Y_J)P_J] - \mu(X_J))]}{E_J [I_J W_J]} - E_J [Y_J - \mu(X_J)] \\ &= \frac{E_J [I_J W_J P_J(1 - 2Y_J)]}{E_J [I_J W_J]} + \left(\frac{E_J [I_J W_J (Y_J - \mu(X_J))]}{E_J [I_J W_J]} - \frac{E_J [Y_J - \mu(X_J)] E_J [I_J W_J]}{E_J [I_J W_J]} \right)\end{aligned}$$

The term in parentheses can be re-written as

$$\begin{aligned}&\frac{E_J [I_J W_J (Y_J - \mu(X_J))] - E_J [(Y_J - \mu(X_J))] E_J [I_J W_J]}{E_J [I_J W_J]} \\ &= \frac{E_J [I_J W_J (Y_J - \mu(X_J))] - E_J [(Y_J - \mu(X_J))] E_J [I_J W_J]}{\sqrt{V_J(I_J W_J) V_J(Y_J - \mu(X_J))}} \frac{\sqrt{V_J(I_J W_J)}}{E_J [I_J]} \times \sqrt{V_J(Y_J - \mu(X_J))} \\ &= \rho_{\tilde{I}(X),Y-\mu(X)} \times \frac{\sqrt{V_J(I_J W_J)}}{E_J [I_J]} \times \sigma_{Y-\mu(X)}\end{aligned}$$

From prior derivations, we then have the desired result.

APPENDIX F. ASYMPTOTIC DERIVATIONS

Here, we take the suggested measures from Arevalo-Rodriguez et al. [2020] which report 87% sensitivity is a reasonable estimates and Cohen et al. [2020] which report 97.6% specificity. This corresponds to a false negative rate of 13% and false positive rate of 2.4%. To allow for potential uncertainty, we assume two *synthetic* simple random samples. The first is a simple random sample of true negative cases denoted S_{FP} ; the second is simple random sample of true positive cases denoted S_{FN} . As μ_t and θ_t are estimated independently at each time t , we can focus on the estimating equations per time point t separately.

Suppose there is a sequence of finite populations of size N_ν indexed by ν . Each finite population has L_ν non-probability samples and probability samples of fixed size n drawn at equally spaced times $\{t'_l\}_{l=1}^L$ over the study window $[0, T]$. Let Δ_ν denote the gap times between consecutive sample times such that as $\nu \rightarrow \infty$ we have that $\Delta_\nu \rightarrow 0$. Finally, let n_{FP} and n_{FN} denote the sample sizes of S_{FP} and S_{FN} respectively. For simplicity, dependency on ν is suppressed and the limiting process is represented by $N \rightarrow \infty$. The asymptotic argument below relies on regularity conditions C1-C6 from Chen et al. [2019], smoothness of the population-level distribution of the time-varying covariates $\{X_{j,t}\}$ as a function of $t > 0$, and smoothness of the propensity function $\pi(x; \theta)$ as a function of $x \in \mathbb{R}^p$.

For each ν and t , the estimates of $\eta = (\mu_t, \theta_t, FP, FN)$ are given by:

$$\Phi(\eta) = \begin{pmatrix} \frac{1}{N} \sum_{j=1}^N I_{j,t} \frac{Y_{j,t} - FP - (1 - FP - FN) \cdot \mu_t}{\pi_{j,t}} \\ \frac{1}{N \times \sum_{l=1}^L K_h(|t - t'_l|)} \sum_{l=1}^L K_h(|t - t'_l|) \left[\sum_{j=1}^N I_{j,t'} X_{j,t'_l} - \sum_{j=1}^N \tilde{I}_{j,t'_l} \tilde{W}_{j,t'_l} \pi_{j,t'_l} X_{j,t'_l} \right] \\ \frac{1}{n_{FP}} \sum_{i=1}^{n_{FP}} \frac{Z_j}{FP} - \frac{1 - Z_j}{1 - FP} \\ \frac{1}{n_{FN}} \sum_{i=1}^{n_{FN}} \frac{\tilde{Z}_j}{FN} - \frac{1 - \tilde{Z}_j}{1 - FN} \end{pmatrix} = \mathbf{0}$$

where $\pi_{j,t'} = \pi(X_{j,t'}; \theta_t)$, Z_j is an indicator of a false positive in the sample S_{FP} and \tilde{Z}_j is an indicator of a false negative in the sample S_{FN} . We assume the $|S_{FP}|^{-1} \sum_{j \in S_{FP}} Z_j = 0.024$ and $|S_{FP}|^{-1} \sum_{j \in S_{FP}} Z_j = 0.30$. Sample sizes, denoted n_{FP} and n_{FN} respectively, are chosen to achieve desired estimator variance, i.e., $\frac{0.024 \cdot (0.976)}{n_{FP}} = \sigma_{FP}^2$ and $\frac{0.13 \cdot 0.87}{n_{FN}} = \sigma_{FN}^2$. In this paper, we set $\sigma_{FP}^2 = 0.02^2$ and $\sigma_{FN}^2 = 0.05^2$ which means $n_{FP} \approx 59$ and $n_{FN} \approx 45$ respectively.

To prove consistency, first consider the setting where a single random sample of size n is observed at time t . Let $\tilde{\Phi}(\eta)$ denote the corresponding estimating equations, which is the same as $\Phi(\eta)$ except for the second component which is now given by

$$\frac{1}{N} \left[\sum_{j=1}^N I_{j,t} X_{j,t} - \sum_{j=1}^N \tilde{I}_{j,t} \tilde{W}_{j,t} \pi_{j,t} X_{j,t} \right].$$

Then under joint randomization of propensity score model and sampling designs, we have $E[\tilde{\Phi}(\eta_0)] = \mathbf{0}$. Consistency then follows by arguments in Section 3.2 of Tsiatis (2006). Under conditions C1-C6 from Chen et al. [2019] and as n increases, we have $\tilde{\Phi}(\hat{\eta}') = 0$ and $\tilde{\Phi}(\eta_0) = O_p(n^{-1/2})$ where $\hat{\eta}'$ here refers to the solution to $\tilde{\Phi}(\eta)$.

To prove consistency under the sequence of sampling regimes, we need to show that $E[\Phi(\eta_0)] \rightarrow 0$ as $N \rightarrow \infty$. First, we study the difference in the 2nd term:

$$\begin{aligned} & \frac{1}{N} E \left[\sum_{j=1}^N \tilde{I}_{j,t} \tilde{W}_{j,t} \pi_{j,t} X_{j,t} - \sum_{l=1}^L \sum_{j=1}^N K_{h,l} \tilde{I}_{j,t'_l} \tilde{W}_{j,t'_l} \pi_{j,t'_l} X_{j,t'_l} \right] \\ &= \frac{1}{N} \sum_{j=1}^N \left[\pi_{j,t} X_{j,t} - \sum_{l=1}^L K_{h,l} \pi_{j,t'_l} X_{j,t'_l} \right], \\ &= \frac{1}{N} \sum_{j=1}^N \left[\sum_{l=1}^L K_{h,l} \pi_{j,t} X_{j,t} \pm \sum_{l=1}^L K_{h,l} \pi_{j,t'_l} X_{j,t} - \sum_{l=1}^L K_{h,l} \pi_{j,t'_l} X_{j,t'_l} \right], \\ &= \frac{1}{N} \sum_{j=1}^N \left[\left(\sum_{l=1}^L K_{h,l} (\pi(X_{j,t}; \theta) - \pi(X_{j,t'_l}; \theta)) \right) X_{j,t} + \sum_{l=1}^L K_{h,l} \pi_{j,t'_l} (X_{j,t} - X_{j,t'_l}) \right], \end{aligned}$$

where $K_{h,l} := K_h(|t - t'_l|) / \sum_{l=1}^L K_h(|t - t'_l|)$ is the normalized kernel for shorthand. The difference in the 1st term is similarly defined.

Let $X_{j,t,l}$ denote the l th component of the vector $X_{j,t}$. Then consider the population-level distribution $\{X_{j,t,l}\}_{j=1}^N$. We make the additional assumption that

$$\lim_{\epsilon \rightarrow 0} \lim_{N \rightarrow \infty} \frac{1}{N} \sum_{j=1}^N X_{j,t+\epsilon,l} = \lim_{N \rightarrow \infty} \frac{1}{N} \sum_{j=1}^N X_{j,t,l}.$$

That is, the limiting distributions are continuous as a function of t . If $\pi(x; \theta)$ is a continuous function in x and under suitable conditions on the kernel density $K_{h_\nu}(\cdot)$ with the bandwidth $h_\nu \rightarrow \infty$ such

that $\sum_{l=1}^L K_{h_\nu}(|t - t'_l|) \rightarrow \infty$ as $\nu \rightarrow \infty$, we have

$$\left| \sum_{l=1}^L K_{h,l} \pi(X_{j,t'_l}; \theta) - \pi(X_{j,t}; \theta) \right| \rightarrow 0$$

Combining this, $E[\Phi(\eta_0) - \tilde{\Phi}(\eta_0)] \rightarrow 0$ which implies consistency as desired.

Then by a first-order Taylor expansion we have $\hat{\eta} - \eta_0 = [\phi(\eta)]^{-1} \Phi(\eta_0) + o_p(\bar{n}^{-1/2})$ where $\phi(\eta) = \partial\Phi(\eta)/\partial\eta$ and $\bar{n} = n \sum_{l=1}^L K_{h,l}$. To calculate

$$\begin{aligned} \frac{\partial\Phi(\eta)}{\partial\mu_t} &= \begin{pmatrix} -\frac{(1-FP-FN)}{N} \sum_{j=1}^N \frac{I_{j,t}}{\pi_{j,t}} \\ 0 \\ 0 \\ 0 \end{pmatrix} \\ \frac{\partial\Phi(\eta)}{\partial\theta_t} &= \begin{pmatrix} -\frac{1}{N} \sum_{j=1}^N I_{j,t} (Y_{j,t} - FP - (1 - FP - FN) \cdot \mu_t) \frac{1 - \pi_{j,t}}{\pi_{j,t}} X_{j,t}^\top \\ -\frac{1}{N} \sum_{t'=1}^T K_{t,t'} \sum_{j=1}^N \tilde{I}_{j,t'} \tilde{W}_{j,t'} \pi_{j,t'} (1 - \pi_{j,t'}) X_{j,t'}^\top \\ 0 \\ 0 \end{pmatrix} \\ \frac{\partial\Phi(\eta)}{\partial FP} &= \begin{pmatrix} -\frac{1}{N} \sum_{j=1}^N I_{j,t} \frac{(1 - \mu_t)}{\pi_{j,t}} \\ 0 \\ -\frac{1}{n_{FP}} \sum_{j=1}^{n_{FP}} \left(\frac{Z_j}{FP^2} + \frac{1 - Z_j}{(1 - FP)^2} \right) \\ 0 \end{pmatrix} \\ \frac{\partial\Phi(\eta)}{\partial FN} &= \begin{pmatrix} -\frac{1}{N} \sum_{j=1}^N I_{j,t} \frac{\mu_t}{\pi_{j,t}} \\ 0 \\ 0 \\ -\frac{1}{n_{FN}} \sum_{j=1}^{n_{FN}} \left(\frac{\tilde{Z}_j}{FN^2} + \frac{1 - \tilde{Z}_j}{(1 - FN)^2} \right) \end{pmatrix} \end{aligned}$$

We are interested in computing $-E \left[\frac{\partial \Phi(\eta)}{\partial \mu_t} \right]^{-1}$ where the expectation is with respect to the random indicators. First, $-E \left[\frac{\partial \Phi(\eta)}{\partial \mu_t} \right]$ is equal to

$$\begin{pmatrix} 1 - FP - FN & \frac{1}{N} \sum_{j=1}^N \zeta_{t,j}(1 - \pi_{j,t})X_{j,t}^\top & 1 - \mu_t & \mu_t \\ 0 & \frac{1}{N} \sum_{t'=1}^T K_{t,t'} \sum_{j=1}^N \pi_{j,t}(1 - \pi_{j,t})X_{j,t}X_{j,t'}^\top & 0 & 0 \\ 0 & 0 & (FP(1 - FP))^{-1} & 0 \\ 0 & 0 & 0 & (FN(1 - FN))^{-1} \end{pmatrix}$$

where $\zeta_{t,j} = (Y_{j,t} - FP - (1 - FP - FN) \cdot \mu_t)$. This matrix can be written as a diagonal matrix equal to the diagonal of $\partial \Phi_n(\eta)/\partial \eta$ and then a rank-three matrix that is zero except for the first row on the off-diagonal. Let $A + B$ denote the sum broken into these 2 components. Then Woodbury matrix identity gives us

$$(A + B)^{-1} = A^{-1} - A^{-1}BA^{-1}$$

In particular, the resulting inverse is of the form

$$\begin{pmatrix} \frac{1}{1 - FP - FN} & b_1 & b_2 & b_3 \\ 0 & \left[\frac{1}{N} \sum_{t'=1}^T K_{t,t'} \sum_{j=1}^N \pi_{j,t}(1 - \pi_{j,t})X_{j,t}X_{j,t'}^\top \right]^{-1} & 0 & 0 \\ 0 & 0 & FP(1 - FP) & 0 \\ 0 & 0 & 0 & FN(1 - FN) \end{pmatrix}$$

where b_1, b_2 , and b_3 can be calculated using the Woodbury identity.

Next, note that $\text{Var}(\Phi(\eta))$ can be decomposed into $A_{1,t} + A_{2,t} + A_{3,t} + A_{4,t}$

$$A_{1,t} = \frac{1}{N} \begin{pmatrix} \sum_{j=1}^N \frac{I_{j,t}(Y_{j,t} - FP - (1 - FP - FN)\mu_t)}{\pi_{j,t}} \\ \sum_{t'=1}^T K_{t,t'} \left[\sum_{j=1}^N I_{j,t'} X_{j,t'} - \pi_{j,t'} X_{j,t'} \right] \\ 0 \\ 0 \end{pmatrix}$$

and

$$A_{2,t} = \frac{1}{N} \begin{pmatrix} 0 \\ \sum_{t'=1}^T K_{t,t'} \left[\sum_{j=1}^N \pi_{j,t'} X_{j,t'} - \sum_{j=1}^N \tilde{I}_{j,t'} \pi_{j,t'} X_{j,t} \right] \\ 0 \\ 0 \end{pmatrix},$$

and

$$A_{3,t} = \begin{pmatrix} 0 \\ 0 \\ \frac{1}{n_{FP}} \sum_{j=1}^{n_{FP}} \frac{Z_j}{FP} - \frac{1-Z_j}{1-FP} \\ 0 \end{pmatrix},$$

and

$$A_{4,t} = \begin{pmatrix} 0 \\ 0 \\ 0 \\ \frac{1}{n_{FN}} \sum_{j=1}^{n_{FN}} \frac{\tilde{Z}_j}{FN} - \frac{1-\tilde{Z}_j}{1-FN} \end{pmatrix},$$

By independence of these components, the variance can be calculated by summation over variance of each term individually yielding. First, $V_{1,t}$

$$N^{-2} \sum_{i=1}^N \begin{pmatrix} \frac{(1-\pi_{j,t})}{\pi_{j,t}} (Y_{j,t} - FP - (1 - FP - FN)\mu_{j,t})^2 & \sum_{t'} K_{t,t'} (1 - \pi_{j,t'}) \zeta_{t',j} X_{j,t'}^\top & 0 & 0 \\ \sum_{t'} K_{t,t'} (1 - \pi_{j,t'}) \zeta_{t',j} X_{j,t} & \sum_{t'} K_{t,t'} \pi_{j,t'} (1 - \pi_{j,t'}) X_{j,t} X_{j,t}^\top & 0 & 0 \\ 0 & 0 & 0 & 0 \\ 0 & 0 & 0 & 0 \end{pmatrix}$$

and $V_{2,t}$ is a block-diagonal matrix with only one non-zero block that is equal to $D_{j,t} = N^{-2} \sum_{t'} K_{t,t'}^2 V_p \left(\sum_{i=1}^n \tilde{W}_{i,t'} \tilde{I}_{i,t'} \pi_{j,t'} X_{j,t'} \right)$ which is the design-based variance-covariance matrix under the probability sampling design; and

$$V_{3,t} = \begin{pmatrix} 0 \\ 0 \\ \frac{1}{n_{FP}} \frac{1}{FP(1-FP)} \\ 0 \end{pmatrix},$$

and

$$V_{4,t} = \begin{pmatrix} 0 \\ 0 \\ 0 \\ \frac{1}{n_{FN}} \frac{1}{FN(1-FN)} \end{pmatrix},$$

The asymptotic variance for the IPW estimator is then the first diagonal element of the matrix $E[\phi_n(\eta_0)]^{-1} \times [V_{1,t} + V_{2,t} + V_{3,t} + V_{4,t}] E[\phi_n(\eta_0)]^{-1}$.

APPENDIX G. IRLS

First derivative with respect to θ

$$\nabla E(\theta) = \sum_{t'=1}^T K_h(|t' - t|) \left[\sum_{j=1}^N I_{j,t'} X_{j,t'} + \sum_{j=1}^N \tilde{W}_{j,t'} \tilde{I}_{j,t'} \pi_t(X_{j,t'}; \theta) X_{j,t'} \right]$$

Second derivative with respect to θ

$$H(\theta) = \sum_{t'=1}^T K_h(|t' - t|) \sum_{j=1}^N \tilde{W}_{j,t'} \tilde{I}_{j,t'} \pi_t(X_{j,t'}; \theta) (1 - \pi_t(X_{j,t'}; \theta)) X_{j,t'} X_{j,t'}^\top$$

Then the Fisher scoring method sets

$$\theta^{(t+1)} = \theta^{(t)} + H(\theta^{(t)})^{-1} \nabla E(\theta^{(t)})$$

APPENDIX H. INDIANA COVID-19 ANALYSIS: ADDITIONAL DETAILS

Table 3 demonstrates minimal bias in the Delphi's COVID-19 Trends and Impact Survey (CTIS) with respect to symptom distributions.

	CTIS			Random
	Lower CI	Estimate	Upper CI	Estimate
Fever	0.073	0.097	0.012	0.018
Cough	0.140	0.150	0.159	0.149
Shortness	0.055	0.062	0.068	0.062

TABLE 3. Comparison of CTIS and random sample restricting CTIS to surveys collected from April 25–29th, 2020.

Next, we describe the two mean-imputation methods.

H.1. **Model 1.** First, we use the pseudo-likelihood to compute the likelihood of contact given age, gender, and test result. Figure 9a and 9b plots the likelihood for 25-34 years old given a negative test and positive test respectfully. We see that the likelihood of COVID-19 is much higher for those with a positive test and the likelihood is time-varying.

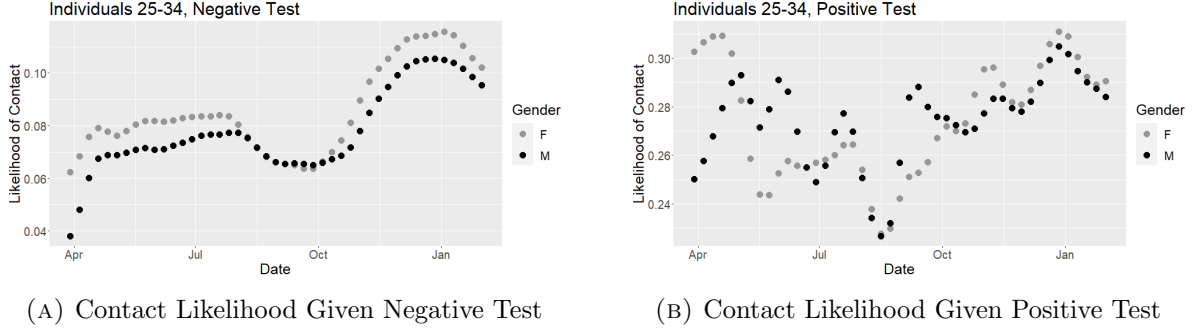


FIGURE 9. Likelihood of COVID-19 contact

We then use the pseudo-likelihood to compute the likelihood of fever given age, gender, COVID-19 contact status and test result. Figure 10a and 10b plots the likelihood for 35-44 year olds given a negative test and positive test respectfully. We see that the likelihood of fever depends heavily on whether they had a COVID-19 contact and their test results. Again, the likelihood is time-varying for most configurations.

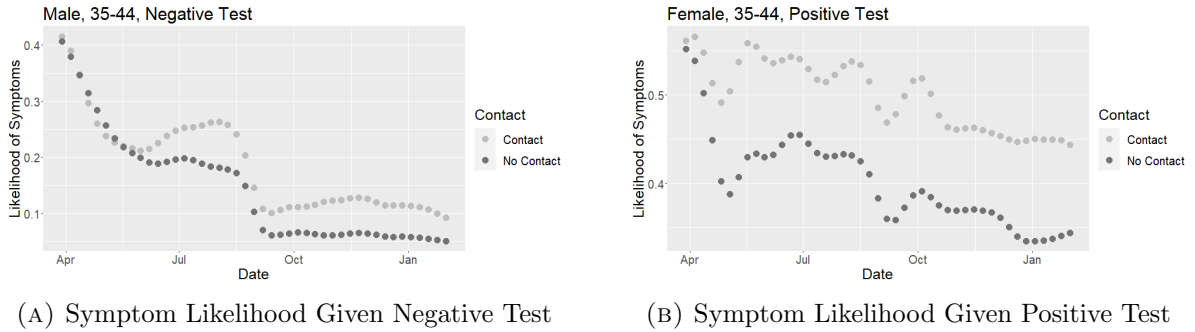
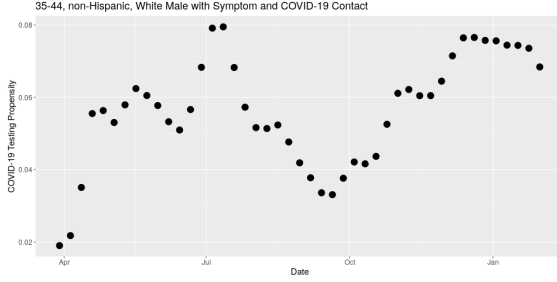


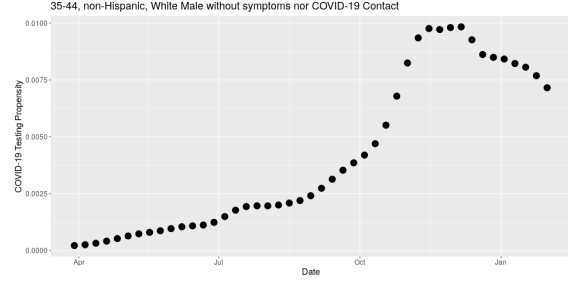
FIGURE 10. Likelihood of reported COVID-19 symptoms

Based on mean-imputation of COVID-19 contact and fever indicators, we can use the proposed pseudo-likelihood approach to compute the likelihood of getting tested for COVID-19 given age, ethnicity, race, gender, fever status, and COVID-19 contact indicator. Figure 11a and 11b plots the likelihood of testing given fever and COVID-19 contact and no fever nor COVID-19 contact

respectfully. We see that the likelihood is time-varying and depends heavily on both fever and COVID-19 contact indicators.



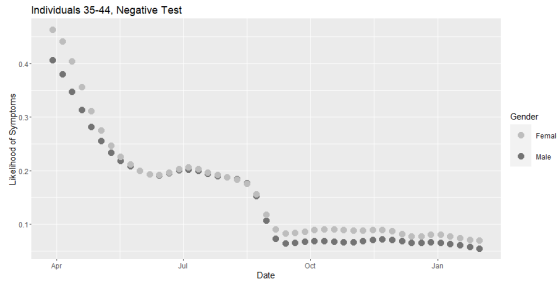
(A) Testing Likelihood Given Fever and COVID-19 Contact



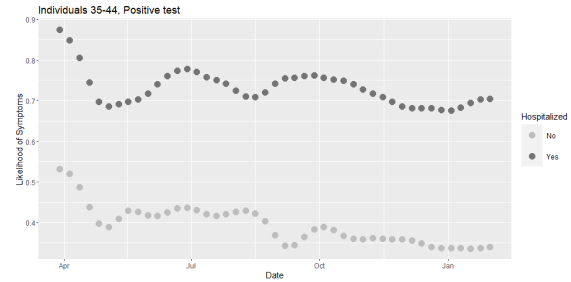
(B) Testing Likelihood Given no Fever nor COVID-19 Contact

FIGURE 11. Testing Likelihood Given no Fever nor COVID-19 Contact

H.2. Model 2 (Hospitalization). This model uses hospitalization records to try and improve our mean-imputation strategy. First, we use the pseudo-likelihood to compute the likelihood of fever given age, gender, and test result. The model only depends on hospitalization status for positive tests. Figure 12a and 12b plots the likelihood for 35-44 years old given a negative test and positive test respectfully. We see that the likelihood of fever is time-varying. For a negative test, the likelihood of ever fever is very high in early April, which accounts for testing restrictions. We see that hospitalization significantly increases the risk of fever given a positive test.



(A) Symptom Likelihood Given Negative Test



(B) Symptom Likelihood Given Positive Test

FIGURE 12. Likelihood of COVID-19 contact

First, we computed the probability of fever given COVID-19 positive test and hospitalization as well as COVID-19 positive test and no hospitalization. We then computed the likelihood of symptom given a COVID-19 positive test by weighting these two likelihoods by the fraction of

COVID-19 positive hospitalizations to COVID-19 total positive cases per week. Mean imputation of fever status for COVID-19 negative tests was performed based on the above model without use of hospitalization data.

Based on mean-imputation of COVID-19 fever using hospitalization records indicators, we can use the proposed pseudo-likelihood approach to compute the likelihood of getting tested for COVID-19 given age, ethnicity, race, gender, and fever status. Figure 6a and 6b in Section 5.1.2 of the manuscript plots the likelihood of testing given fever and no fever respectfully for all age ranges. We see that the likelihood is time-varying and depends heavily on both fever status.

H.2.1. Propensity plots. Here we present the testing propensity for four strata: (1) non-Hispanic, white female, (2) non-Hispanic, African American male, (3) Hispanic, White male, and (4) Hispanic male who selects ‘Some other Race’. Strata (1) presented in Figure 13 demonstrates a small gender difference in testing propensities. Strata (2) and (3) presented in Figures 14 and 15 demonstrates a lower rate of testing among African Americans and Hispanic white men compared to non-Hispanic, white men respectively (approximately 2 times lower). Strata (4) presented in Figure 16 demonstrates a much higher testing rate for Hispanic men who select “Some Other Race”.

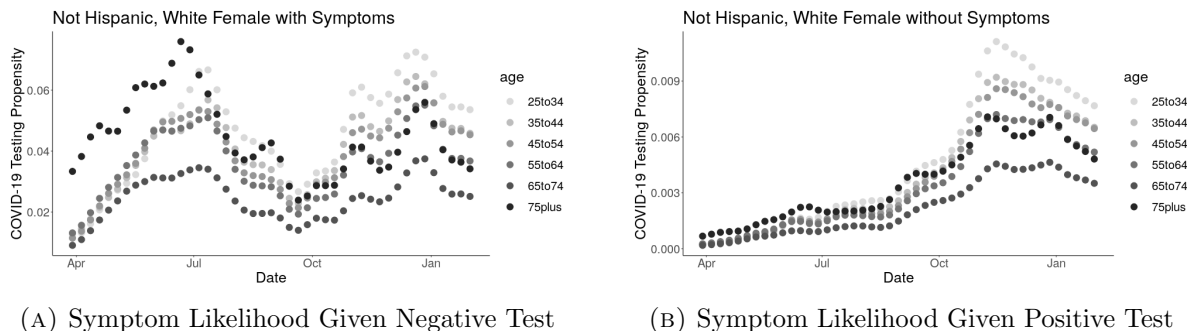


FIGURE 13. Likelihood of COVID-19 contact for Non-Hispanic, White Females

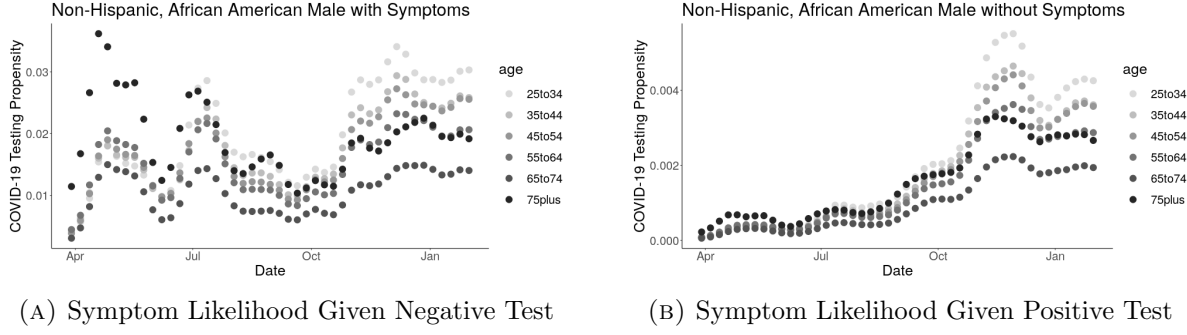


FIGURE 14. Likelihood of COVID-19 contact for Non-Hispanic, African American Males

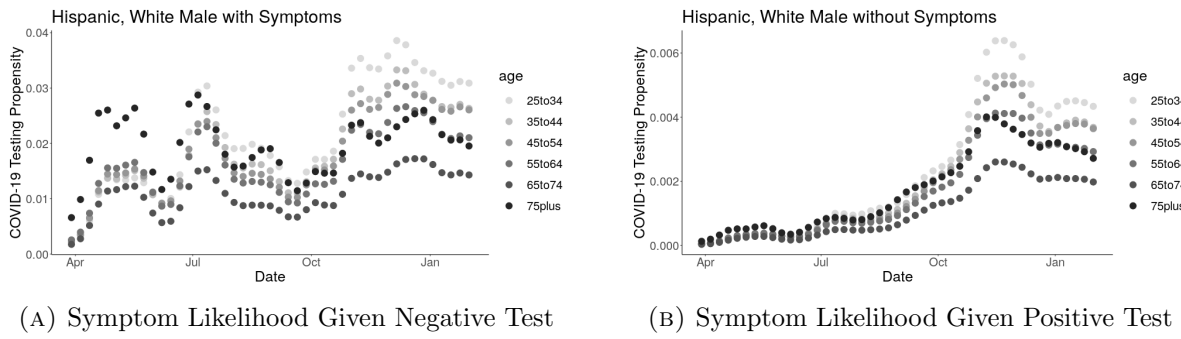


FIGURE 15. Likelihood of COVID-19 contact for Hispanic, White Males

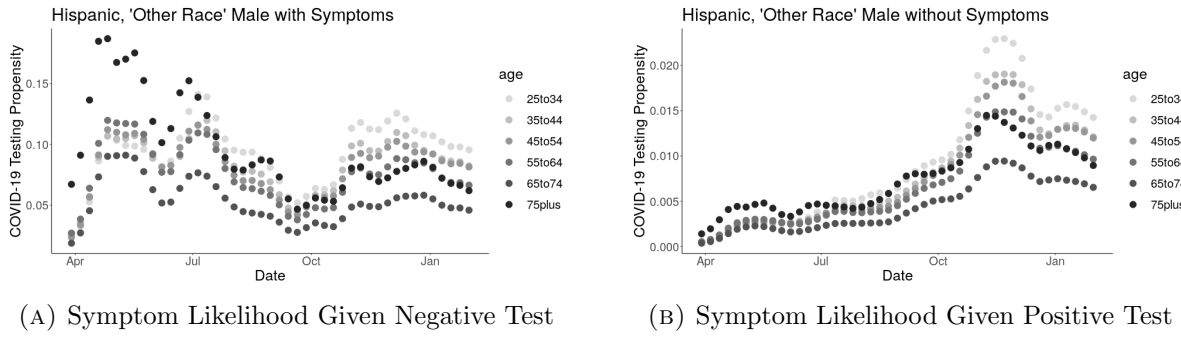


FIGURE 16. Likelihood of COVID-19 contact for Hispanic, Males who select 'Some Other Race'.

H.2.2. *Confidence Intervals.* Figure 17 in the supplementary materials presents the confidence intervals per time point for the IPW2 estimator. The confidence interval length decreases substantially over time, reflecting the increased testing capacity. Due to the number of surveys per week, under correct model specification there is minimal uncertainty in the parameter estimates. As the number of tests per week increases to over one hundred thousand, there is minimal uncertainty in the active

infection rate estimates. This points to the importance of the statistical decomposition (4.4) and the discussion in Section 4.1.2.

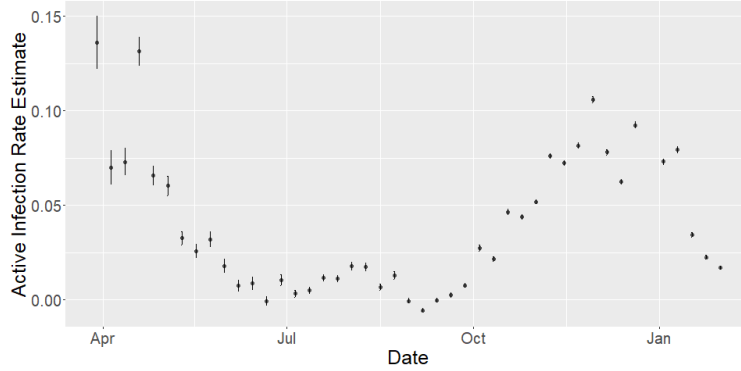


FIGURE 17. IPW2 estimate with confidence intervals

APPENDIX I. MODEL-BASED: PRIOR SPECIFICATION

For simplicity, we list the priors used in STAN below:

- $\text{beta} \sim \text{Normal}(1.5, 1) \text{ T}[0,];$
- $\text{gamma} \sim \text{normal}(0.3, 0.5) \text{ T}[0,];$
- $\text{sigma} \sim \text{normal}(0.4, 0.5) \text{ T}[0,];$
- $\text{phi_inv} \sim \text{exponential}(5);$
- $\text{i0} \sim \text{normal}(0, 10);$
- $\text{e0} \sim \text{normal}(0, 10);$
- $\text{eta} \sim \text{normal}(1, 1) \text{ T}[0,];$
- $\text{eta_two} \sim \text{normal}(1, 1) \text{ T}[0,];$
- $\text{eta_three} \sim \text{normal}(1, 1) \text{ T}[0,];$
- $\text{nu} \sim \text{exponential}(1./5);$
- $\text{nu_two} \sim \text{exponential}(1./5);$
- $\text{nu_three} \sim \text{exponential}(1./5);$
- $\text{xi_raw} \sim \text{beta}(1, 1);$
- $\text{phi} = 1/\text{phi_inv};$
- $\text{xi} = \text{xi_raw} + 0.5;$

where `beta`, `eta`, `eta_two`, `eta_three` refer to the four values that form the time-varying parameter β_t when combined with `xi`, `eta`, `eta_two`, `eta_three` in the SEIR model as described in Section 4.2. Following Song et al. [2020], we employ Runge-Kutta (RK4) approximations for discretization. Due to the low number of deaths per strata, i.e., based on Race, Age, Sex and Ethnicity, we employ a kernel smoothing of the new infections per age strata into these sub-strata using relative number of observed deaths. This ensured a suitably complex model that fits the observed death data well while generating strata-specific active infection rates that can be used in the doubly-robust estimation procedure.

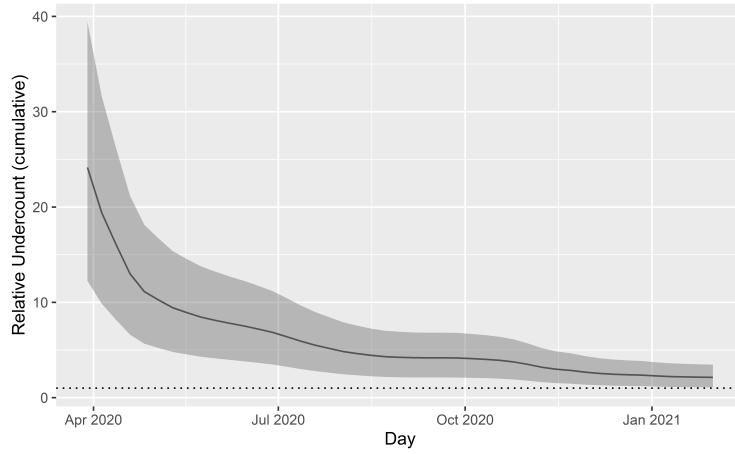


FIGURE 18. Cumulative undercount based on SEIR model

Figure 18 is a plot of undercount based on the SEIR model. We plot relative undercount on a cumulative basis since January due to the case counts reflecting active infections. Figure 19 is a sensitivity analysis of the active infection rate under SEIR model with 10% increase and decrease in the average IFR. We see that the impact on the doubly robust estimates is minimal. A floor based on weekly case count divided by the Indian population size is also presented.

APPENDIX J. ALTERNATIVE ESTIMATOR OF THE INSTANTANEOUS REPRODUCTIVE NUMBER

Here we present estimates of the instantaneous reproductive number using the approach of Cori et al. [2013] under the SEIR model from Section 3.3. Let I_t denote the total infectiousness of infected individuals at time t . Then $E[I_t] = R_t \sum_{s=1}^t I_{t-s} w_s$ where w_u is the infectivity function. Here, we follow Cori et al. [2013] and choose a discretized shifted Gamma distribution with mean

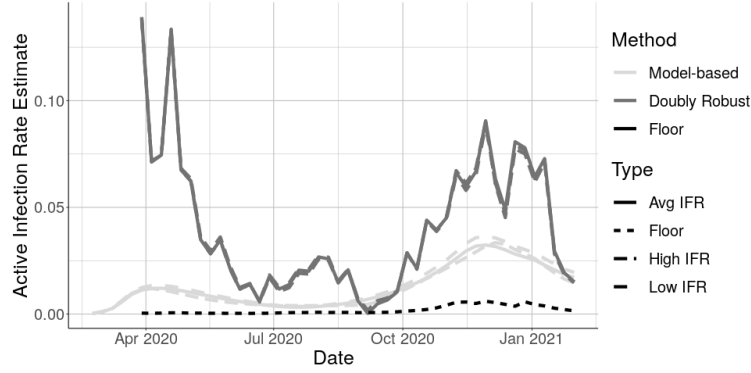


FIGURE 19. Model-based and Doubly Robust active infection rate estimates under Irons and Raftery [2021] marginal IFR estimate of 0.84%, under a 10% higher marginal IFR of 0.924%, and under a 10% lower marginal IFR of 0.756%.

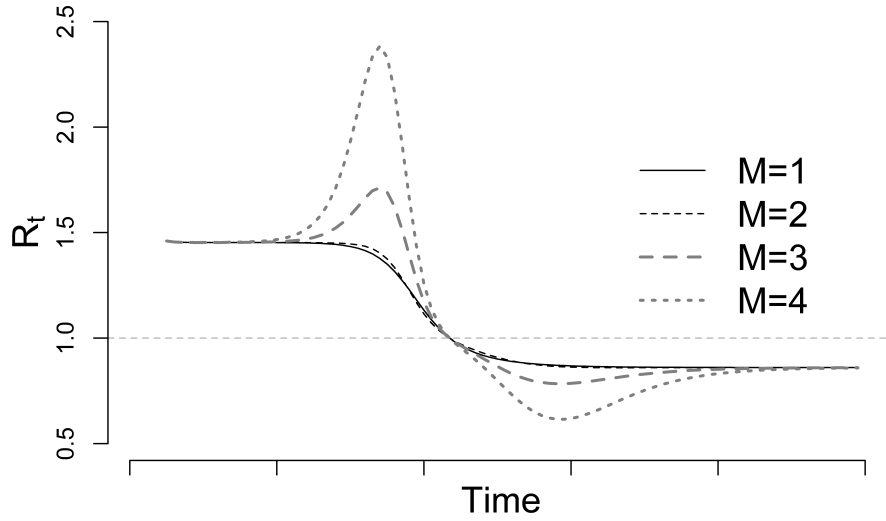


FIGURE 20. Effective reproductive rate estimator

FIGURE 21. Potential bias in instantaneous reproductive rate estimator based on Cori et al. [2013] under an SEIR model with $\beta = 1.2$, $\gamma = 0.15$, and $\sigma = 0.3$. Here, $f = 0.02$, $FP = 0.024$, $FN = 0.13$, and a range of relative sampling fractions $M = f_1/f_0$ are considered.

7 days and standard deviation 2 days. Then a moment-based estimator can be obtained by $\hat{R}_t = I_t / \sum_{s=1}^t I_{t-s} w_s$, which takes the form of the ratio estimators in Section 3.2. Therefore, the bias can be readily obtained from the associated Taylor series decomposition, with the terms related to time $t - 1$ replaced by a weighted version.

Figure 21 presents the potential bias in instantaneous reproductive rate estimator. The general conclusions follow similarly as in Figure 4a. The rate is overestimated prior to the peak and underestimated afterwards. Estimates at the peak time appear to have minimal bias.

APPENDIX K. SENSITIVITY ANALYSIS TO UNMEASURED CONFOUNDING

The proposed approach relies on the assumption $I_{j,t}^{(NR)} \perp\!\!\!\perp Y_{j,t} \mid X_{j,t}$, i.e., the sampling indicator in the non-probabilistic survey is conditionally independent of the outcome given the covariates. However, estimates of population quantities based on inverse-weighting and/or model-based estimates will be biased in the presence of ‘unobserved confounding’. Here we introduce a sensitivity analysis to address this concern. To this end, we consider the logit-linear model by Imbens [2003], adjusted to the time-varying, self-selection setting from the single time-point, causal inference setting. That is, consider the model

$$\text{logit}\pi(I_t = 1 \mid x_t, u_t) = h_t(x_t) + \alpha_t u_t$$

$$E[Y_t \mid i_t, x_t, u_t] = l_t(x_t) + \delta_t u_t$$

for functions h_t and l_t that depend on time. Re-arranging terms we have

$$E[Y_t \mid i_t, x_t, u_t] = l_t(x_t) + \frac{\delta_t}{\alpha_t} (\text{logit}\pi(I_t = 1 \mid x_t, u_t) - h_t(x_t))$$

The key idea in Imbens [2003] is that positing a distribution on $\pi(I_t = 1 \mid x_t, u_t)$ directly allows one to circumvent the need to specify a distribution for U_t , a highly non-trivial task.

The logit-linear model above unfortunately does not lead to a tractable sensitivity analysis. Instead, we consider a sensitivity model based on work by Veitch and Zaveri [2020], again adjusted to deal with the current setting of self-selection, given by

$$\begin{aligned} \pi_t(X_t, U_t) &\sim \text{Beta}(\pi_t(X_t)(1/\alpha_t - 1), (1 - \pi_t(X_t))(1/\alpha_t - 1)) \\ I_t \mid X_t, U_t &\sim \text{Bern}(\pi(X_t, U_t)) \\ \rho_t(X_t, U_t) &= Q_t(X_t, 1) + \delta_t (\text{logit}\pi_t(X_t, U_t) - \mathbb{E}[\text{logit}\pi_t(X_t, U_t) \mid X_t, I_t = 1]) \\ Y_t \mid I_t, X_t, U_t &\sim \text{Bern}(\rho_t(X_t, U_t)), \end{aligned} \tag{K.1}$$

where $Q_t(X_t, 1)$ is the conditional expectation of the outcome given covariates X_t and self-selection into the nonprobability sample, i.e., $I_t = 1$. The time-varying sensitivity parameter $\alpha_t \in (0, 1)$ controls the influence of the unobserved confounder U_t on selection propensity. In particular, α_t measures the change in belief of how likely an individual self-selects into the non-probabilistic sample at time t :

$$\alpha_t = E[\pi_t(X_t, U_t)|I_t = 1] - E[\pi_t(X_t, U_t)|I_t = 0].$$

The sensitivity model satisfies the requirement that the self-selection propensity and conditional expectation outcome model can match the observed data:

$$P(I_t = 1|X_t) = E[E[I_t|X_t, U_t]|X_t] = E[\pi_t(X_t, U_t)|X_t] = \pi_t(X_t)$$

$$E[Y_t|X_t, I_t = 1] = E[E[Y_t|X_t, U_t, I_t = 1]|X_t, I_t = 1] =: Q_t(1, X_t).$$

Moreover, the model satisfies that Y_t does not depend on I_t given (X_t, U_t) . This is a key adaptation to the non-probabilistic survey setting with potential time-varying confounding and a binary outcome.

IPW estimator: By assumption, observing X_t and U_t together leads to consistent estimation via the estimator:

$$\begin{aligned} \mathbb{E} [\pi_t^{-1}(X_{J,t}, U_{J,t}) I_{J,t} Y_{J,t}] &= \mathbb{E}[E[Y_{J,t}|X_{J,t}, U_{J,t}]] \\ &= \mathbb{E}[Q(1, X_{J,t}) + \delta_t (\text{logit}\pi_t(X_{J,t}, U_{J,t}) - \mathbb{E}[\text{logit}\pi_t(X_{J,t}, U_{J,t})|X_{J,t}, I_{J,t} = 1])] \end{aligned}$$

IPW-based estimator: Investigating the IPW estimator using only X_t , we have:

$$\begin{aligned} \mathbb{E} [\pi_t^{-1}(X_{J,t}) I_{J,t} Y_{J,t}] &= \mathbb{E} \left[\frac{\pi_t(X_{J,t}, U_{J,t})}{\pi_t(X_{J,t})} \pi^{-1}(X_{J,t}, U_{J,t}) I_{J,t} Y_{J,t} \right] \\ &= \mathbb{E} \left[\frac{\pi_t(X_{J,t}, U_{J,t})}{\pi_t(X_{J,t})} \mathbb{E}[Y_{J,t}|X_{J,t}, U_{J,t}] \right]. \end{aligned}$$

Using the fact that $\mathbb{E}[\pi_t(X_{J,t}, U_{J,t})|X_{J,t}] = \pi_t(X_{J,t})$, the *bias* is

$$\delta_t \mathbb{E} \left[\text{logit}\pi_t(X_{t,J}, U_{t,J}) - \frac{\pi_t(X_{J,t}, U_{J,t})}{\pi_t(X_{J,t})} \text{logit}\pi_t(X_{t,J}, U_{t,J}) \right].$$

Using the fact that $Z \sim \text{Beta}(\alpha, \beta)$ then $E[\ln(Z)] = \psi(\alpha) - \psi(\alpha + \beta)$, $E[\ln(1 - Z)] = \psi(\beta) - \psi(\alpha + \beta)$ then $E[\text{logit}(Z)] = \psi(\alpha) - \psi(\beta)$ where ψ is the digamma function. Moreover, $\mathbb{E}[Z \ln Z] =$

$\frac{\alpha}{\alpha+\beta} [\psi(\alpha+1) - \psi(\alpha+\beta+1)]$ and

$$\begin{aligned}\mathbb{E}[(1-Z)\ln(1-Z)] &= \frac{\beta}{\alpha+\beta} [\psi(\beta+1) - \psi(\alpha+\beta+1)] \\ \mathbb{E}[\ln(1-Z)] &= [\psi(\beta) - \psi(\alpha+\beta)] \\ \Rightarrow -\mathbb{E}[Z\ln(1-Z)] &= \frac{\beta}{\alpha+\beta} [\psi(\beta+1) - \psi(\alpha+\beta+1)] - [\psi(\beta) - \psi(\alpha+\beta)].\end{aligned}$$

and thus

$$\begin{aligned}\mathbb{E}[Z\text{logit}(Z)] &= \frac{\alpha}{\alpha+\beta} [\psi(\alpha+1) - \psi(\alpha+\beta+1)] + \frac{\beta}{\alpha+\beta} [\psi(\beta+1) - \psi(\alpha+\beta+1)] \\ &\quad - [\psi(\beta) - \psi(\alpha+\beta)] \\ &= \psi(\alpha+\beta) - \psi(\alpha+\beta+1) + \frac{\alpha}{\alpha+\beta} [\psi(\alpha+1) - \psi(\beta+1)] + \frac{1}{\beta} \\ &= \frac{\alpha}{\alpha+\beta} [\psi(\alpha+1) - \psi(\beta+1)] + \left[\frac{1}{\beta} - \frac{1}{\alpha+\beta} \right].\end{aligned}$$

Plugging in $\alpha = \pi_t(X_t)(1/\alpha_t - 1)$ and $\beta = (1 - \pi_t(X_t))(1/\alpha_t - 1)$ yields:

$$\pi_t(X_{t,J}) \left[\psi \left(\pi_t(X_{t,J}) \left(\frac{1-\alpha_t}{\alpha_t} \right) + 1 \right) - \psi \left((1 - \pi_t(X_{t,J})) \left(\frac{1-\alpha_t}{\alpha_t} \right) + 1 \right) \right] + \frac{\alpha_t}{1-\alpha_t} \frac{\pi_t(X_{t,J})}{1 - \pi_t(X_{t,J})}.$$

Since $\pi_t(X_t)$ cancels with the denominator term, the first term will match the form of the $E[\text{logit}(Z)]$ and therefore using the fact that $\psi(x+1) = \psi(x) + 1/x$, we can write the bias simply as

$$-\delta_t \frac{\alpha_t}{1-\alpha_t} \mathbb{E} \left[\frac{1}{\pi_t(X_{t,J})} \right]$$

Note that this is an expectation over the population. Thus, estimation requires use of the probabilistic sample in order to estimate the potential bias.

K.1. Reparametrization. Following Veitch and Zaveri [2020], we re-express the outcome-confounder strength in terms of the partial coefficient of determination

$$R_t^2(\alpha_t, \delta_t) = \frac{\mathbb{E}[(Y_{J,t} - Q_t(1, X_{J,t}))^2 | I_{J,t} = 1] - \mathbb{E}[(Y_{J,t} - \mathbb{E}[Y_{J,t} | X_{J,t}, U_{J,t}])^2 | I_{J,t} = 1]}{E[(Y_{J,t} - Q_t(1, X_{J,t}))^2 | I_t = 1]}$$

in terms of δ_t^2 . To do so, write

$$\begin{aligned}
& \mathbb{E}[(Y_{J,t} - \mathbb{E}[Y_{J,t}|X_{J,t}, U_{J,t}])^2 | I_{J,t} = 1] \\
&= \mathbb{E}[(Y_{J,t} - Q_t(1, X_{J,t}))^2 | I_{J,t} = 1] \\
&\quad - 2\delta \mathbb{E}[(Y_{J,t} - Q_t(1, X_{J,t}))(\text{logit}\pi(X_{J,t}, U_{J,t}) - \mathbb{E}[\text{logit}\pi(X_{J,t}, U_{J,t}) | X_{J,t}, I_{J,t} = 1]) | I_{J,t} = 1] \\
&\quad + \delta^2 \mathbb{E}[(\text{logit}\pi_t(X_{J,t}, U_{J,t}) - \mathbb{E}[\text{logit}\pi_t(X_{J,t}, U_{J,t}) | X_{J,t}, I_{J,t} = 1])^2 | I_{J,t} = 1] \\
&= \mathbb{E}[(Y_{J,t} - Q_t(1, X_{J,t}))^2 | I_{J,t} = 1] - \delta^2 \mathbb{E}[\text{var}(\text{logit}\pi_t(X_{J,t}, U_{J,t}) | X_{J,t}, I_{J,t} = 1)]
\end{aligned}$$

By Beta-Bernoulli conjugacy, the second term is the variance of the logit-transformed Beta distribution which has an analytic expression:

$$\text{var}(\text{logit}\pi_t(X_{J,t}, U_{J,t}) | X_{J,t}, I_{J,t} = 1) = \psi_1(\pi(X_{J,t})(\alpha_t - 1) + 1) + \psi_1((1 - \pi(X_{J,t}))(1/\alpha_t - 1))$$

where ψ_1 is the trigamma function. This implies the following relationship:

$$(K.2) \quad R_t^2(\alpha_t, \delta_t) = \delta_t^2 \frac{\mathbb{E}[\psi_1(\pi(X_{J,t})(\alpha_t - 1) + 1) + \psi_1((1 - \pi(X_{J,t}))(1/\alpha_t - 1)) | I_{J,t} = 1]}{E[(Y_{J,t} - Q_t(1, X_{J,t}))^2 | I_{J,t} = 1]}$$

Note that unlike the prior expectation, these are expressed conditional on self-selection, i.e., $I_{J,t} = 1$.

This was done since the binary outcomes are only measured in the non-probabilistic sample.

Following from [Veitch and Zaveri, 2020, Theorem 5], the parameter α_t can be re-expressed as

$$(K.3) \quad \alpha_t = 1 - \frac{\mathbb{E}[\pi(X_{t,J}, U_{t,J})(1 - \pi(X_{t,J}, U_{t,J}))]}{\mathbb{E}[\pi(X_{t,J})(1 - \pi(X_{t,J}))]},$$

which is a more convenient form when trying to estimate the parameter from observed data.

K.2. Calibration of sensitivity parameters. Based on (K.2) and (K.3), one can use the probability and nonprobability samples to calibrate the sensitivity parameters to be in line with the observed covariate influence on treatment and outcome. That is, for a given observed covariate $Z_{J,t}$, we wish to measure the degree of influence it has on self-selection and outcome given the other observed covariates $X_{J,t} \setminus Z_{J,t}$. Note that this dependence is likely time-varying, which is why it is important that α_t and R_t^2 are functions of time t .

For the outcome, we can measure the partial coefficient of determination as:

$$R_{t,Z}^2 := \frac{\frac{1}{n} \sum_{i=1}^n (y_{i,t} - \hat{Q}_{t,Z}(1, x_{i,t} \setminus z_{i,t}))^2 - \frac{1}{n} \sum_{i=1}^n (y_{i,t} - \hat{Q}_t(1, x_{i,t}))^2}{\frac{1}{n} \sum_{i=1}^n (y_{i,t} - \hat{Q}_{t,Z}(1, x_{i,t} \setminus z_{i,t}))^2},$$

where \hat{Q}_t is the conditional expectation given all covariates and $\hat{Q}_{t,Z}$ is the conditional expectation given all covariates except Z . Note these are sums averages the non-probabilistic sample. We can measure influence of Z on self-selection propensity given $X_{J,t} \setminus Z_{J,t}$ by

$$\hat{\alpha}_{t,Z} := 1 - \frac{\sum_{j=1}^N I_{j,t}^R W_{j,t}^R \cdot \hat{\pi}(X_{J,t})(1 - \hat{\pi}(X_{J,t}))}{\sum_{j=1}^N I_{j,t}^R W_{j,t}^R \cdot \hat{\pi}(X_{J,t} \setminus Z_{J,t})(1 - \hat{\pi}(X_{J,t} \setminus Z_{J,t}))}$$

where $\hat{\pi}_t(\cdot)$ is the fitted self-selection probability based on (4.2) in Section 4.1.1 using the appropriately chosen set of observed covariates.

K.3. IPW Sensitivity Analysis of COVID-19 Active Infection Prevalence in Indiana.

Here we perform a sensitivity analysis of the IPW estimator of COVID-19 active infection prevalence in Indiana. While Veitch and Zaveri [2020] use Austen plots, we do not have such a simple visualization due to time-dependence. Here, we plot $\alpha_{t,Z}$ and $R_{t,Z}^2$ as functions of time for three covariates that demonstrate different patterns: (1) Symptoms, (2) Race, and (3) Ethnicity. Figures 22a and 22b present these “calibration curves.” Figure 22c presents the bias under these three curves. Here, we see that if an unobserved confounder has similar strength in selection-confounder and outcome-confounder relationships as “Symptom Status”, then bias would be high even into early 2021. However, bias under an unobserved confounder with similar strength to “Ethnicity” dissipates significantly by late 2020.

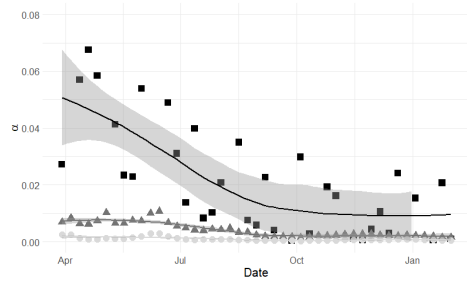
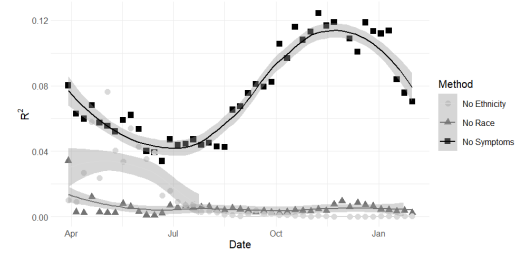
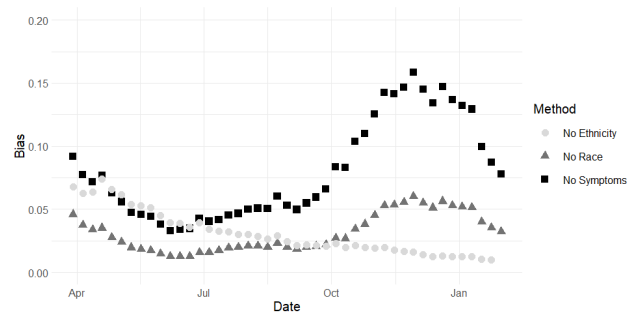
(A) Calibration curves for α per week(B) Calibration curves for R^2 per week(C) Bias as a function of α and R^2 calibration curves

FIGURE 22. Sensitivity analysis for time-varying active infection rate estimates